Master of Science Thesis in Electrical Engineering
Department of Electrical Engineering, Linköping University, 2021

Modeling and Automatic Control of a Seedbed Tine Harrow

Viktor Uvesten and Henrik Fallgren

LINKÖPING UNIVERSITY

Master of Science Thesis in Electrical Engineering

Modeling and Automatic Control of a Seedbed Tine Harrow

Viktor Uvesten and Henrik Fallgren

LiTH-ISY-EX--21/5390--SE

Supervisor: **Daniel Arnström**
ISY, Linköpings universitet
Jakob Lindberg
"The company"

Examiner: **Fredrik Gustafsson**
ISY, Linköpings universitet

Division of Automatic Control
Department of Electrical Engineering
Linköping University
SE-581 83 Linköping, Sweden

Abstract

The agricultural industry is facing a major technological change with autonomous vehicles in focus. This follows the global trend, where the interest lies in increasing production, while reducing costs with the help of automation. Considering the vast amount of different agricultural machines on the market today, the process of automating these machines is long and needs to start on one machine. This thesis covers the process of developing an automatic control system for a seedbed tine harrow.

The seedbed tine harrow cultivates the soil at a certain depth in preparation for planting. The different functions on the harrow are today manually controlled from the cab of the tractor, which means that the farmer must constantly monitor the process. The proposed control system uses radar sensors to measure and hydraulic systems to control the harrowing depth and the crossboards. The development of the control system consists of modeling the harrow, creating a simulation environment, choosing a filtering strategy, and testing different control algorithms.

The resulting control algorithm, implemented and tested on the harrow, consisted of a Kalman filter with separate PD-controllers for each function, the harrowing depth, and the angle of the crossboards. The crossboard controllers use an additional feedforward control from measured disturbance. The thesis also explores a set of experimental control algorithms, for instance, cascade control. These are not possible to implement on this generation of the harrow but show promising potential from simulation.

Acknowledgments

During the writing of this thesis, we have had the opportunity to meet and work with several people that we would like to thank, both from the Company, which provided us with the project, and Linköping University. It has been an eventful spring and despite the pandemic, dangerous weather, and disease the project has followed the schedule thanks to these people.

First of all, we want to thank our supervisor at the Company, Jakob Lindberg for assistance with testing and for sharing his knowledge about the harrow, hydraulics, and farming in general. We also want to show our appreciation to Dan Person from Syncore for the help with programming and implementing the control system on the harrow.

We would like to thank our supervisor at the university Daniel Arnström. Your willingness to assist us with ideas and feedback through the spring has been motivating and appreciated. We would like to thank our examiner Fredrik Gustavsson for support and guidance through the project.

Lastly, we want to thank our opponents, Mattias Granström and Johanna Heide. They have contributed with motivation and feedback during the spring, and without them, the project would not have been the same.

Linköping, May 2021
Viktor Uvesten and Henrik Fallgren

Contents

Notation

Variables

Notation	Meaning
s	Laplace-transform variable
z	$\mathcal{Z}$-transform variable
p	The derivation opperator
q	The forward shift operator

Operators

Notation	Meaning
$\hat{x}_{n\|m}$	Estimation of state x in time step n given the information from time step m

Abbreviations

Abbreviations	Meaning
PID	Proportional, integral, differential (regulator)
KF	Kalman filter
LP-filter	Low pass filter
CB	Crossboard
CBF	Crossboard front
CBR	Crossboard rear

1

Introduction

Figure 1.1: *Overview of the tine harrow.*

1.1 Problem Formulation

1.1.1 Motivation

In this thesis, the possibility to produce a robust control strategy for a tine harrow, shown in Figure 1.1, will be investigated. Currently, the different functions of the harrow are controlled from the tractor cab manually and require constant super-

vision. The goal is to be able to create an autonomous system working predictably and desirably to ease the workload and strive towards a fully autonomous system.

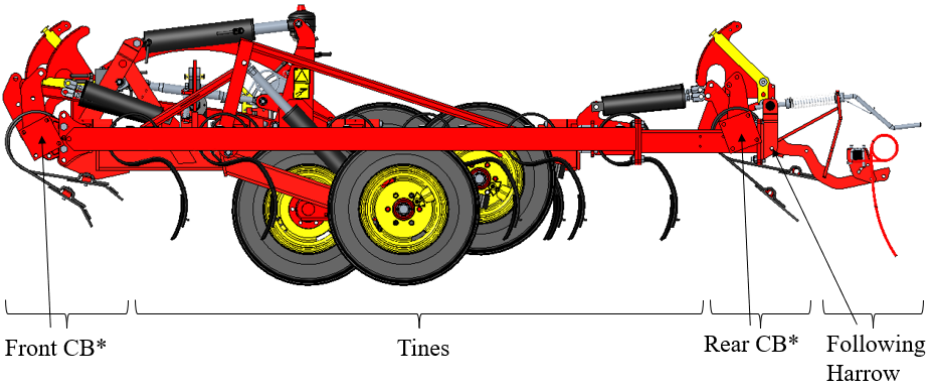

Figure 1.2: *A side view of the tine harrow*
**Crossboards are linear over the entire width of the machine unlike the figure shows.*

1.1.2 Purpose

The farming industry is facing a major technological revolution where the main goal is to automate the harrowing process and get rid of the need for supervision from a farmer. This will result in increased efficiency and profit for the farmer and is the reason why the company[1] is striving to automate its wide range of agricultural machinery. The tine harrow has been in the company's production line since the 70s and has continuously been developed through the years into, among others, the tine harrow model focused on in this report. The next step in development is to automate the main functions, the working depth, and crossboard intensity. The performance of the harrow is dependent on the soil quality, weather, and other disturbances. Therefore, the farmer constantly needs to monitor the process and tune the machine if needed. Using radar sensors the depth and crossboard intensity can be estimated and then used in an automatic control system to ensure that the harrow performs proficiently.

1.1.3 Problem Statement

Questions covered by this thesis are:

- How advanced does a model of the real system need to be in order to design a robust control system?

[1] This thesis is done towards an agricultural company. Because some components and technology are at an early development stage the company will, however, only be referred as *the company* and not its real name.

- What measurements are necessary and how should these be filtered to suit the control system?
- What control strategy is most suitable for this application considering the development cost, system characteristics, and robustness with respect to measurement noise and model errors?

1.1.4 Delimitations

The control system will be developed to control an already existing product and will not be designed with other products in mind. This means that the three existing control functions can not be modified and the thesis will not focus on the development of these hardware components.

1.2 Seedbed Tine Harrow

A seedbed tine harrow is used to loosen up, level, and cultivate the soil in preparation for planting. The harrow, which the thesis is covering, comes in different setups depending on the customer's demand. In Figure 1.2 the three components which are working the soil are displayed, the two main components which come as standard are the front crossboard and the tines.

The crossboard is used to level the field and destroy bigger chunks of soil by pushing a wall of soil in front of the harrow. The work intensity is controlled by adjusting the angle of the crossboard. The rear crossboard works in the same way as the front and is an addition which further levels the soil.

The tines, which are the black "hooks" underneath the harrow in Figure 1.2, are used to cultivate the soil, and are designed like springs which enables them to flex back when digging into the soil. This causes the tines to vibrate during the harrowing and moves larger aggregates to the top and smaller clusters to the bottom which is a desirable distribution for optimal growth. The front crossboard and tines during work are shown in Figure 1.3.

The crossboards and the height of the harrow, which sets the depth of the tines, are controlled by hydraulic cylinders. Each component is driven by three cylinders which are series-connected and are dimensioned in a way that provides synchronized movement.

1.3 Related Work

The possible applications and benefits of automatic control in agricultural machinery was recognized already twenty years ago [14]. Even if the applications seemed possible at the time, there have not been many agricultural companies that have delivered machines using automatic control since then. Even the research in the area has been limited and in 2020 a number of researchers concluded that "...very few researchers have focused on application of control algorithms for agriculture related practices" [13].

Figure 1.3: *The tines and crossboard working together to level and cultivate the soil.*

Even though the research on this topic is limited, some papers exist where the possibilities of controlling the tillage depth are researched. In [7] the possibility of controlling the depth of a rotary tillage machine was investigated with promising results. In [15] researchers developed a control system for the working depth of a seed drill. Here they used a cascade control with the stroke of the hydraulic cylinder as the secondary loop. In this article, they used the optimal PID-tuning rule from [2]. This tuning rule is developed with regard to integrated processes in agricultural applications, which is also relevant for this work.

The big difference between the works mentioned and this project is the extent of the control system. The control systems mentioned control one function of the machine, usually the tillage depth, using several different sensors, while this thesis will focus on multiple dependent functions, harrowing depth, and crossboard wall heights, using only one type of radar sensor.

2

Modelling and Simulation

This chapter describes the system and the process of developing motion models and a simulation environment.

2.1 System Overview

In order to design a desirable control system without large-scale testing, the characteristic of each controllable component needs to be described mathematically. This is done using drawings of, and tests on, the harrow. The harrow has up to three controllable components which are the front and rear crossboard and the wheel axle, see Figure 1.2. The crossboards are varied by changing the angle of attack against the soil. Increasing the angle results in the crossboard digging deeper into the soil and creating a more perpendicular angle between soil and crossboard. This results in an increased work intensity which builds a bigger wall in front of the crossboard, shown and explained in more detail in Figure 2.1. The position of the wheel axle sets the height of the entire harrow, thus affecting all components. The main purpose of changing the height is to vary the working depth of the tines where a lower height results in the tines penetrating the soil deeper. Because all components are affected by the height, the work intensity of the crossboards also increases by lowering the height. The depth of the tines and the height of each wall are the variables to be controlled.

The components are controlled by separate hydraulic systems. Each hydraulic system contains three or four series-connected cylinders which control one of the three functions of the harrow. The three functions of the harrow are design in similar ways. The generic mechanics of all three functions can be seen in Figure 2.2. The input signal u moves the hydraulic cylinder length L_c which then rotates a pivot arm. This rotation θ is then mechanically translated to a movement of the function, which in turn results in a change in an angle of attack or a height y. This

will be further explained in section 2.3.

Figure 2.1: *The crossboard shoving a wall of soil in front. By rotating the beam on which the crossboard is mounted the work intensity is adjusted. Pushing the crossboard against the soil creates higher intensity as a result of crossboard depth and angle between soil and crossboard.*

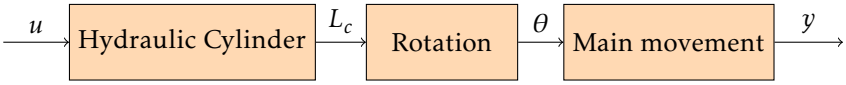

Figure 2.2: *Generic diagram of the mechanics of each of the functions, where u is the input signal, L_c is the length of the cylinder, θ is the rotation of the pivot arm, y is the output either a angle of attack or the harrow height.*

2.1.1 Hydraulic System

The hydraulic systems of the harrow are designed using a "master-slave" setup. This setup guarantees that cylinders spread across the harrow work synchronously even if the load affecting the harrow is uneven. The cylinders for each component are connected in series, four cylinders for the motion of the front crossboard and three for the motion of the rear crossboard and the height of the harrow. The synchronized motion is accomplished by dimensioning the cylinders in such a way that two connected chambers have the same piston area, this is illustrated in Figure 2.3.

The hydraulic cylinders get oil pressure from the internal pump of the tractor. The flow of the oil is controlled by two "2 way normally closed, proportional flow control valve" for each function, one to control the flow to the upper chamber and one to control the flow to the lower chamber. The valves are fed with a controlled

current and the flow of oil can be closely approximated to be proportional to this controlled current as $q_v = K_v(i - i_0)$, where q_v is the flow from the valve, K_v is the valve gain, i is the provided current and i_0 is the opening current. The approximation can be seen in Figure 2.4.

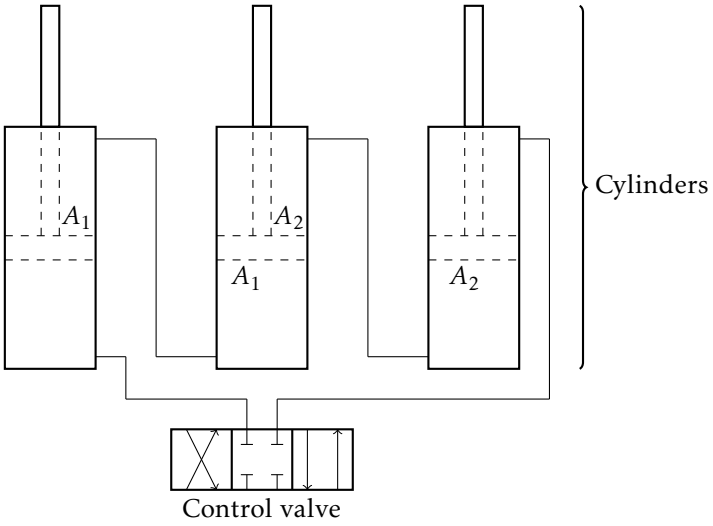

Figure 2.3: *Illustration of a "master-slave" cylinder setup. Equal piston area in two connected chambers allows for synchronized movement.*

2.2 Modeling Theory

To be able to model and simulate the harrow some theoretical background is needed.

2.2.1 Model Estimation of Hydraulic System

In contrast to the mechanics of the motion of the harrow, the hydraulic system has several unknown characteristics that are hard to estimate from drawings and technical documentation. Therefore the hydraulics of the system is modeled using system identification.

System Identification

System identification is about estimating parameters, $\bar{\theta}$, in a proposed model structure $\hat{G}(p, \bar{\theta})$ to best fit measured data of the system [10]. The measured data is the input signal $u(t)$ and the output signal $y(t)$. This gives that for each $u(t)$ in the measured data, the proposed model will give an estimate of the output

$$\hat{y}(t|\bar{\theta}) = \hat{G}(p, \bar{\theta})u(t) \tag{2.1}$$

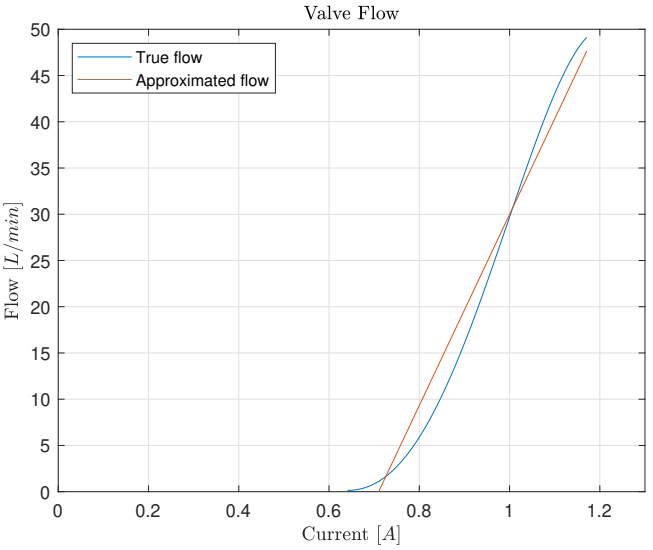

Figure 2.4: *The flow as a function of applied current. It shows the true flow and a comparison to a true proportional flow. It also shows the dead-zone of the system, i.e the opening current* i_0, $0 - 0.64A$.

where p is the differential operator and $\hat{y}$ is the estimated value of the output. From this the prediction error is defined as:

$$\epsilon(t, \bar{\theta}) = y(t) - \hat{y}(t|\bar{\theta}). \tag{2.2}$$

Using this prediction error for every measurement $t = 1, 2, ..., N$, the following performance measure can be created

$$V_N(\bar{\theta}) = \frac{1}{N} \sum_{t=1}^{N} \epsilon^2(t, \bar{\theta}). \tag{2.3}$$

This measure indicates how well the estimated model using $\bar{\theta}$ predicts the true model. Naturally, the goal is to find

$$\bar{\theta}^* = \arg\min_{\bar{\theta}} V_N(\bar{\theta}), \tag{2.4}$$

i.e the parameters that best fit the data in terms of minimizing the cost function V_N.

Proposed Model Structure

In order for (2.4) to estimate the true system $G^0(p)$, the proposed model needs to have the right order of the differential equation. This can be achieved either

by using the known information about the system and setting up a proposed differential equation. It is also possible to propose a higher-order model and let the algorithm find the best suiting parameters. These two techniques are called grey-box and black-box modeling respectively. A drawback of black-box modeling is that the algorithm takes longer to find an optimum and might fit the model to the sensor noise thus giving an bad model.

Since there is prior knowledge about the hydraulic system, the best approach is to use a grey box model.

The hydraulic cylinder is controlled by the proportional valve which controls the flow of hydraulic oil. As shown in Figure 2.4, this flow can be approximated as linear.

$$q = K_v i_c, \tag{2.5}$$

where q is the flow through the valve, and K_v is the valve gain. Furthermore, $i_c = i(t) - i_0$ where i_0 is the dead zone of the valve and $i(t)$ is the controlled current. The flow into the cylinder gives the following equation:

$$q = Av_c + K_\beta \dot{v}_c, \tag{2.6}$$

where A is the area of the cylinder chamber which the fluid flows to, seen in Figure 2.5,v_c is the piston speed, and $K_\beta \dot{v}_c$ is to describe the compression of the fluid in the system. Combining (2.5), (2.6) and applying the Laplace transform gives:

$$V_c(s) = \frac{K_v}{(A + sK_\beta)} I(s). \tag{2.7}$$

The measured data from the hydraulic system is the input current $i(t)$ and the output is the cylinder length $L_c(t) = L_s(t) + L_{c0}$. Therefore, the (2.7) need to be integrated to describe the change of stroke

$$L_s(s) = \frac{K_v}{s(A + sK_\beta)} I(s). \tag{2.8}$$

Combining the parameters and adding a time delay T_d to the system gives the final model

$$L_s(s) = \frac{K}{s(1 + sT)} e^{-sT_d} I(s), \tag{2.9}$$

with the model parameter $\bar{\theta} = [K, T, T_d]$. This is commonly referred to as a first order lag plus integral plus delay (FOLIPD) process model [2].

2.3 Modeling

2.3.1 Overview

The model of the harrow has been divided into three parts where each part describes the relationship between a control signal and a system output. These parts are:

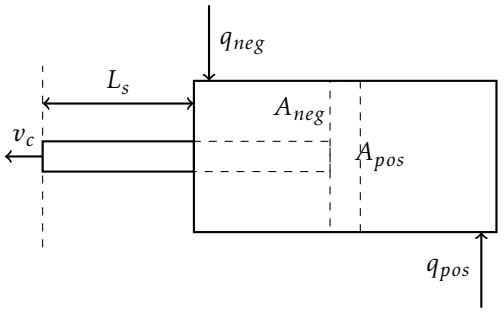

Figure 2.5: *Generic diagram of a hydraulic cylinder. q_{neg} is the flow for negative movement, q_{pos} is the flow for positive movement, A_{neg} and A_{pos} is the area of which the hydraulic oil pushes for each direction.*

- Crossboard Front
- Harrow Height
- Crossboard Rear

Each model is structured as: A controlled current steers a hydraulic proportional valve which creates a flow of hydraulic oil. This flow moves the hydraulic cylinder with a speed proportional to the flow which rotates a pivot arm. These rotations finally translate to a motion for each model. In order to obtain these mathematical models, measurements and testing on the harrow have been carried out, and drawings of the harrow have been used.

2.3.2 Hydraulic Cylinder

The hydraulic cylinders were modeled using measurements from the harrow together with the proposed model in (2.9). The measurements were done by measuring the applied current to the valve, compensated for the opening current i_0, as well as the stroke of the cylinder with a linear potentiometer. Data from the measurements can be seen in Figure 2.6.

Using the collected data together with System Identification Toolbox [8] in MATLAB the optimal parameters $\bar{\theta}$ that minimized the cost function in (2.4) were obtained. The result showed that the model could estimate the true system fairly well, with small deviations at some speeds. The resulting model with estimation and validation data is shown in Figure 2.7

The hydraulic cylinders are asymmetrical, which means that they will have different dynamic properties if they are contracting or expanding. This is solved by dividing the model into two parts one for positive (expanding) and one for negative (contracting) movements.

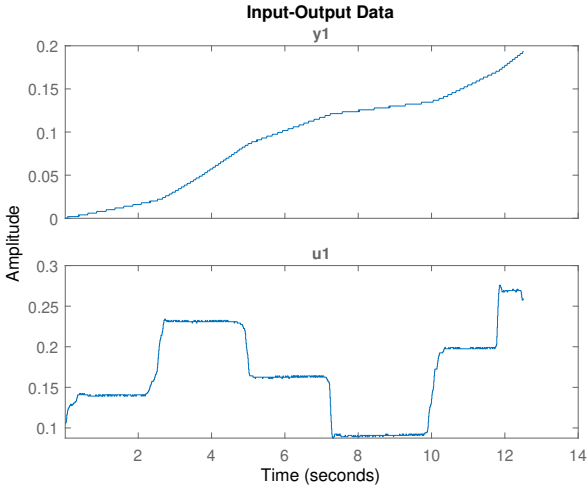

Figure 2.6: *Measured data from the hydraulic system of the crossboard front. The data y_1 is the cylinder stroke L_s, while u_1 is the applied current i.*

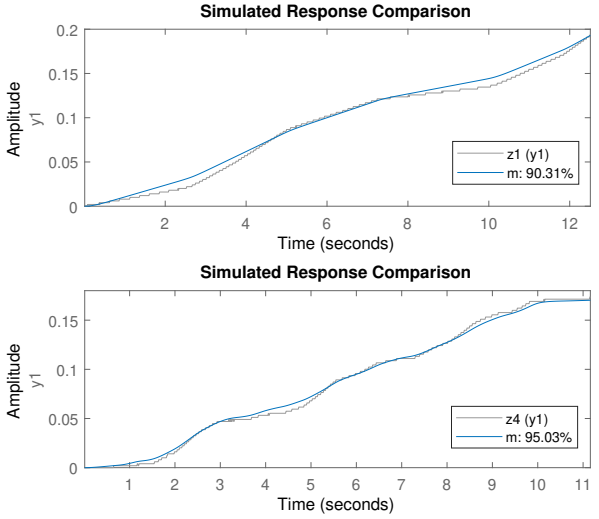

Figure 2.7: *Estimated hydraulic model of front crossboard. z_1 is the data used for estimation, z_4 is validation data, m is the estimated model output.*

The resulting model constants from the System Identification toolbox are shown in Table 2.1

Table 2.1: *Model constants for hydraulic cylinders*

Model:	**Direction**	K	T	T_d
CB front	*Pos*	0.094981	0.16	0.01
CB front	*Neg*	0.074141	0.02	0.19
Harrow Height	*Pos*	0.057597	0.10	0.07
Harrow Height	*Neg*	0.078936	0.02	0.07
CB rear	*Pos*	0.117950	0.01	0.05
CB rear	*Neg*	0.107020	0.18	0.04

2.3.3 Rotational Dynamics

As the hydraulic cylinder moves, it pivots a rotational arm, as seen in Figure 2.8. This rotation can be described as a function from the length of the cylinder L_c to an angle on the pivot arm θ. This mechanism is the same on all three models, but the dimensions are different.

Figure 2.8: *The hydraulic set up on the harrow. The picture shows CB front*

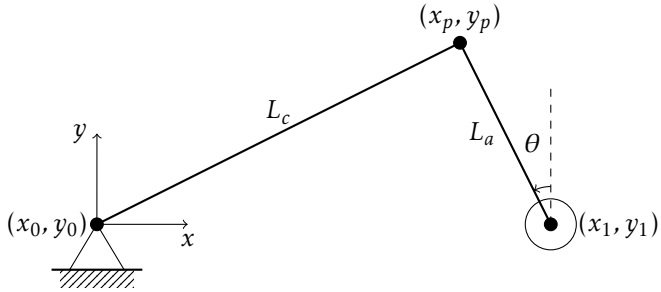

Figure 2.9: *Diagram of the rotational motion. L_c is the cylinder length, L_a is the length of the rotational lever and θ is the rotation.*

From the mechanical diagram in Figure 2.9, the following equations can be produced.

$$x_1 - L_a \sin(\theta) = x_p \tag{2.10}$$

$$y_1 + L_a \cos(\theta) = y_p \tag{2.11}$$

$$\sqrt{(x_p - x_0)^2 + (y_p - y_0)^2} = L_c \tag{2.12}$$

Equations (2.10), (2.11), (2.12) together with the fact that $(x_0, y_0) = (0, 0)$ gives the following equation:

$$(x_1 - L_a \sin(\theta))^2 + (y_1 + L_a \cos(\theta))^2 = L_c^2 \tag{2.13}$$

Rewriting (2.13) gives the angle θ as a function of L_c.

$$\theta = \sin^{-1}\left(\frac{x_1^2 + y_1^2 + L_a^2 - L_c^2}{2L_a\sqrt{x_1^2 + y_1^2}}\right) + \tan^{-1}\left(\frac{y_1}{x_1}\right) \tag{2.14}$$

Linear Assumptions

In control design, it is often desirable to have linear models. Equation (2.14) is nonlinear, but as it turns out, the equation can be approximated as linear, which will be useful when designing the control system. For small angles of θ the angular velocity ω can be approximated as a function of the piston speed v_c as

$$\dot{\theta} = \omega \approx \frac{-v_c}{L_a}. \tag{2.15}$$

Using (2.15) and the initial angle θ_0, the linear approximation can be used to compute the approximated angle $\hat{\theta}$. The comparison between the approximation and the actual angles for the three models are shown in Figure 2.10, 2.11, and 2.12.

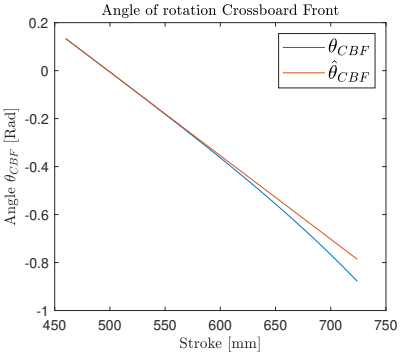

Figure 2.10: *Comparison between θ_{CBF} and $\hat{\theta}_{CBF}$.*

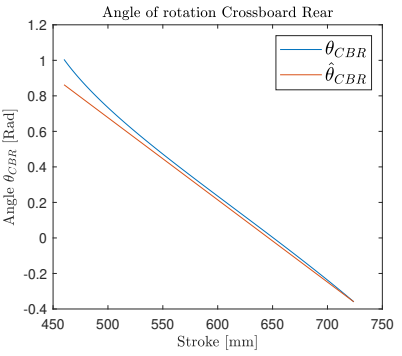

Figure 2.11: *Comparison between θ_{CBR} and $\hat{\theta}_{CBR}$.*

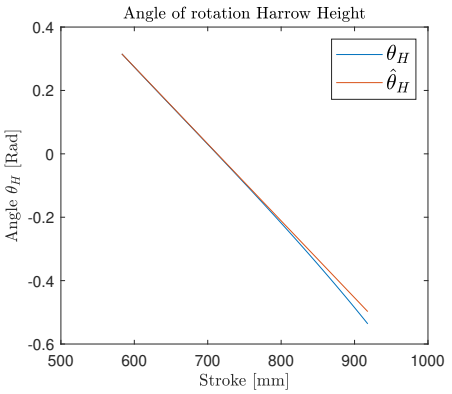

Figure 2.12: *Comparison between θ_h and $\hat{\theta}_h$.*

From Figure 2.10 - 2.12 it can be concluded that (2.15) can approximate (2.14) fairly well across the whole stroke of the cylinder. Worth noticing is that (2.15) approximates with higher precision at some intervals, and this interval coincides with the working point θ_W for the different functions ($\theta_{W,CBF} \approx 570$mm, $\theta_{W,CBR} \approx 560$mm, and $\theta_{W,h} \approx 670$mm).

2.3.4 Harrow Depth

The height of the harrow is controlled by an axle with two rigid arms, L_a and L_w, illustrated in Figure 2.13. The hydraulic cylinder is connected to (x_p, y_p) and the wheel suspension to (x_w, y_w). When the cylinder extends, the wheel arm is lowered and the height is increased.

The height of the harrow is mainly controlled to set a working depth for the tines. The height is calculated from a point on the underside of the frame and l_{ax} is the length from this point to the rotating axis. The depth d_{tine} is simply

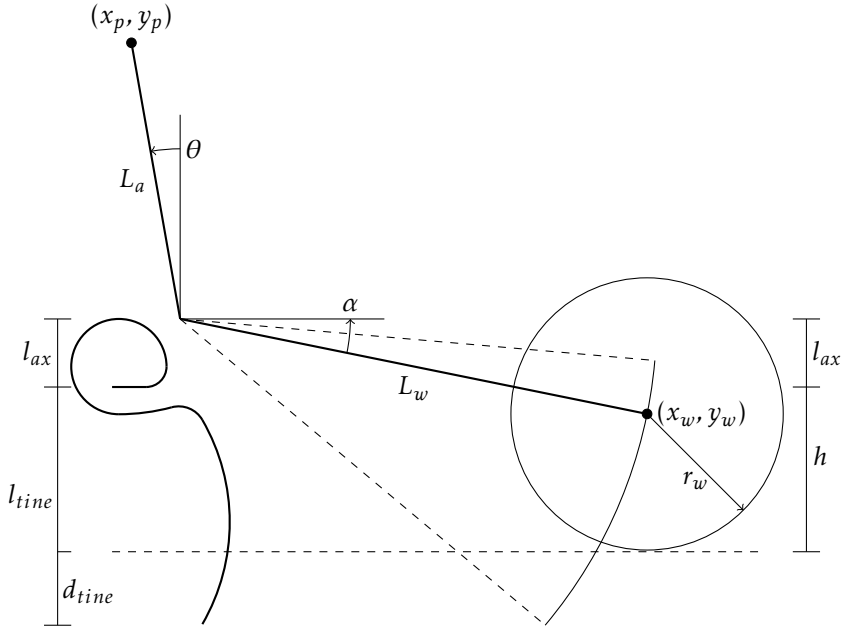

Figure 2.13: *Replication of the arms controlling the height of the harrow.*

calculated by comparing the height of the harrow, including the radius of the wheels r_w, to the length of the tines. α_0 is the angle of the wheel arm L_w when $\theta = 0$. Using (2.16) the angle of the wheel arm α can be calculated for any given θ. The deepest working depth is obtained when the hydraulic cylinder is fully compressed resulting in θ obtaining its highest possible value.

$$\alpha = \alpha_0 - \theta \tag{2.16}$$

$$h = L_w \cdot \sin(\alpha) + r_w - l_{ax} \tag{2.17}$$

$$d_{tine} = l_{tine} - h \tag{2.18}$$

Tine Dynamics

The tines on the harrow are constructed to spring back in order to vibrate and cultivate the soil. When the depth d_{tine} increases, the length of a tine l_{tine} decreases as a result of this spring back. The tine dynamics are modeled in a black-box fashion using measurement on the harrow. The resulting model is

$$l_{tine} = \begin{cases} l_{tine,0} - \frac{K_{tine}}{pT_{tine}+1}(l_{tine,0} - h), & \text{if}(l_{tine,0} - h) > 0 \\ l_{tine,0} & \text{otherwise} \end{cases} \tag{2.19}$$

where $l_{tine,0}$ is the initial length of the tine, K_{tine} is the model gain, and T_{tine} is the time constant.

2.3.5 Crossboard

The variable that needs to be controlled for the crossboards is the height of the wall of soil that builds up in front of the crossboard. The wall is dependent on the the angle of attack and depth that the crossboard penetrates the soil. These variables are in turn dependent in the angle of rotation from (2.14).

Crossboard Front

The crossboard in front has an attack angle of 0° when the hydraulic cylinder is fully contracted, which means that the angle of attack α is dependent on the angle of rotation θ as well as the initial angle θ_0. The mechanics of the crossboard are shown in Figure 2.14 and the equations that describe the front crossboard are

$$\alpha = \alpha_0 - \theta \tag{2.20}$$

$$d_{CBF} = L_{CBF} \cos(\alpha) - h_{CBF}. \tag{2.21}$$

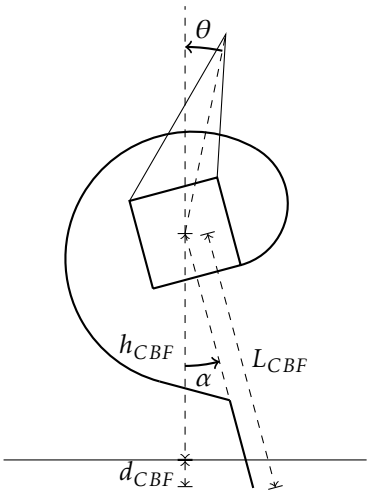

Figure 2.14: *Mechanical diagram of the front crossboard where θ is the rotation angle, h_{CBF} is the height above ground, α is the angle of attack, L_{CBF} is the length of the crossboard, and d_{CBF} is the working depth.*

Crossboard Rear

The rear crossboard has mirrored movement compared to the front. When the hydraulic cylinder is fully contracted the angle of attack is at its minimum. The mechanics of the crossboard are shown in Figure 2.15 and the equations of the movement are

$$\alpha = \alpha_0 + \theta \tag{2.22}$$
$$\beta = \beta_0 + \alpha \tag{2.23}$$
$$d_{CBR} = L_{CBR}\cos(\beta) - h_{CBR}. \tag{2.24}$$

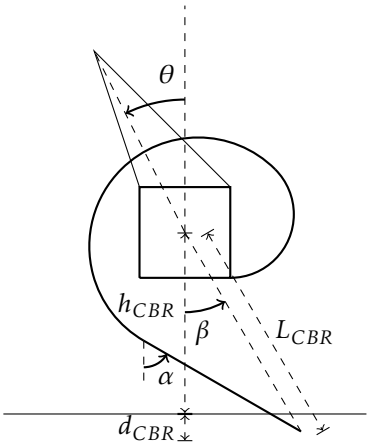

Figure 2.15: *Mechanical diagram of the rear crossboard where θ is the rotation angle, h_{CBR} is the height above ground, α is the angle of attack,β is the crossboard angle, L_{CBF} is the length of the crossboard, and d_{CBR} is the working depth.*

Soil Wall

The wall of soil that builds up against the crossboard needs to be modeled in order to simulate the system and design a controller that accurately controls this wall. The biggest problem with modeling this wall is that the dynamics is depending on several unknown parameters, such as the composition of the soil, humidity of the soil, and the speed of the harrow. Instead of doing extensive work with modeling and estimating unknown parameters in a grey-box fashion, a black-box model for the dynamics is estimated using measurements from runs of the system.

Since it is known that the wall builds up by shoving the soil, and that the wall height increases by lowering the crossboard, it can be assumed that the wall is directly dependent on the crossboard working depth d_{CB}. It can also be assumed that the system reaches a steady state if there is no influence of external disturbances. Given these assumptions the wall can be modeled using a differential equation, most commonly expressed as a transfer function [11]

$$w_{CB} = G_w(p)d_{CB}, \tag{2.25}$$

where w is the height of the wall and G_w is the transfer function. The most basic approach to model this system is to assume the transfer function is a first order

system

$$w_{CB} = \frac{K_w}{T_w p + 1} d_{CB}. \tag{2.26}$$

But observing the real system shows some overshoots in the wall height, which is not possible with a first order system. Using an experimental identification method, the wall dynamics could be modeled using a second order system with a zero as

$$w_{CB} = \frac{a_2 p + a_1}{b_3 p^2 + b_2 p + b_1} d_{CB}, \tag{2.27}$$

where the constants $a_{1,2}$ and $b_{1,2,3}$ are determined to achieve a static gain between 4 and 6, rise time between 3 and 5 seconds and an overshoot of about 20%. Worth noting is that these parameters do not have to be exact, this is because of the uncertainty in the dynamics and that the controller needs to be able to control an arbitrary wall.

2.3.6 State Space Models

Many popular control strategies such as LQ controllers, require a linear state space model [9]. In order to use such control strategies the nonlinear equations need to be linearized. This is done around a given working point where the harrow usually operates.

Depth model

Combining (2.9), (2.15), (2.16), (2.17) and (2.18) with states $x_1(t) = d$, $x_2(t) = \dot{d}$, and the control signal $u(t) = i(t)$, the linearized state space model for the depth is

$$\dot{x}_1 = x_2 \tag{2.28a}$$

$$\dot{x}_2 = \frac{-1}{T} x_2 - \frac{L_w \cos(\alpha_0 - \theta_0) K}{T L_a} u, \tag{2.28b}$$

where θ_0 is the working point of the linearization.

Crossboard Model

The crossboard model is more advanced than the depth model and it is thus more difficult to linearize. Using (2.9), (2.15), (2.20) and (2.21) together with (2.26), instead of (2.27) for simplicity, with the states, $x_1 = w_{CBF}$, $x_2 = \theta_{CBF}$, $x_3 = \dot{\theta}_{CBF}$, the control signal $u(t) = i(t)$ and with the disturbance $v(t) = h_{CBF}$, the nonlinear state space model of the front crossboard is expressed as

$$\dot{x}_1 = \frac{-1}{T_w} x_1 + \frac{K_w L_{CBF}}{T_w} \cos(\alpha_0 - x_2) - \frac{K_w}{T_w} v \tag{2.29a}$$

$$\dot{x}_2 = x_3 \tag{2.29b}$$

$$\dot{x}_3 = \frac{-1}{T} x_3 - \frac{K}{T L_{a,CBF}} u. \tag{2.29c}$$

In the same way, with (2.9), (2.15), (2.22), (2.23) and (2.24) together with (2.26) the nonlinear state space model of the rear crossboard is expressed as

$$\dot{x}_1 = \frac{-1}{T_w} x_1 + \frac{K_w L_{CBR}}{T_w} \cos(\alpha_0 + \beta_0 + x_2) - \frac{K_w}{T_w} v \tag{2.30a}$$

$$\dot{x}_2 = x_3 \tag{2.30b}$$

$$\dot{x}_3 = \frac{-1}{T} x_3 - \frac{K}{T L_{a,CBR}} u. \tag{2.30c}$$

2.4 Simulation and Validation

When producing a control system for the first time, a lot of testing and calibrating is required. Real-world testing is expensive and takes a lot of time, especially when big machines, such as harrows, are used. Therefore, being able to simulate tests is essential for efficiency and cost. With this in mind a simulation environment of the harrow was established in Simulink. Simulink is a tool created for modelling and simulation of dynamic systems. The ability to use it together with MATLAB creates a combination of textual and graphical programming which is helpful in this kind of work.

2.4.1 Implementation

The movement of the different components was implemented using (2.16)-(2.24) from above, where θ is given by (2.14). The cylinders was modeled in Simulink according to Figure 2.16. The control signal u is a current sent to the control valve controlling the cylinders. The dead zone and the saturation represents the dead zone and the maximum current of the valve. Depending on whether the signal is positive or negative the cylinder extends or contracts. The characteristics of the movement was implemented as described in (2.9) using parameters produced in Chapter 2.3.2. To get cylinder movement the signal is integrated.

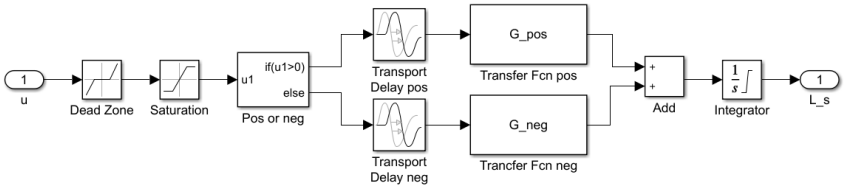

Figure 2.16: *Implemented cylinder model in Simulink for extension and contraction dependent on control signal u.*

For a complete overview of the entire system implemented in Simulink, see Appendix A.

2.4.2 Disturbances

Disturbances created by varying soil hardness as well as an uneven surface are random and in order to get an accurate model, these have to be simulated as well. The disturbances affecting the height and the crossboards differ a lot and were therefore generated differently in the simulation environment.

Height

To determine the characteristics of the disturbances data from previous testing, presented in Figure 2.18, was used. The data shows a large underlying disturbance with a rather constant period of approximately 4 seconds. On top of this two higher frequency disturbances were apparent, one with a frequency of 3-4 Hz and one smaller with an even higher frequency of 20 Hz. Using these observations the disturbance affecting the height could be modelled. To ensure that all modelled sensors had a similar behaviour a single random signal representing the large disturbance was used. This signal was split into four signals with different time delays to mimic the placements of the sensors. An offset was added to each signal as well as the two higher frequency disturbances which gave each signal different attributes. The resulting disturbance is presented in Figure 2.19.

Crossboards

The crossboard disturbances can be separated in three parts: harrow movement, uneven soil and measurement errors. According to (2.21), (2.24) and (2.27) the wall height is dependent on the height of the harrow, thus the changing harrow height can be seen as a measurable disturbance. Due to the considerable length of the harrow, soil quality is not constant across the harrow. This implicates that the wall height at each sensor will be different and is modeled with a randomly slowly changing offset for each sensor. The changing soil quality is modeled by adding slow changing noise to the wall height from (2.27). Lastly, to simulate the measurement noise, white independent noise is added to the simulated signal.

2.4.3 Validation

To ensure that the implemented model behaves in the same way as the real system, data from simulations are compared with data collected from the system.

System Validation

The model controlling the height was validated using a simple test where a control signal was sent to the control valve for a sett amount of time. This was made both ways while standing still on flat ground to eliminate any disturbances. The same test was performed in Simulink and the results are compared in Figure 2.17.

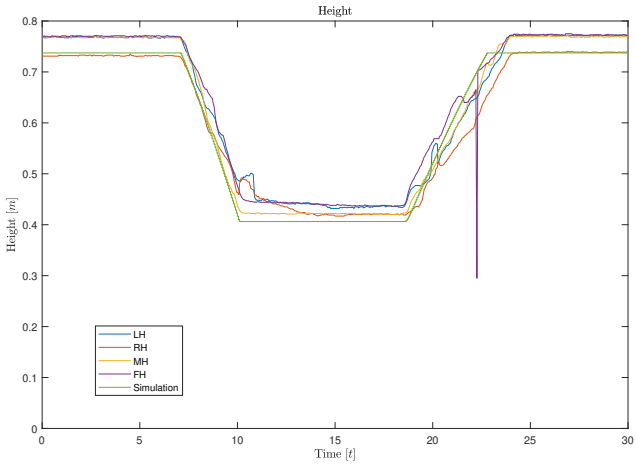

Figure 2.17: *Comparison of simulated model and real system, the green straight line represents the simulation and the others the real test. LH, RH, MH, and FH are the different sensors measuring the height of the harrow.*

Disturbance Validation

The measured and the simulated data are presented in Figure 2.18 and 2.19. Because the disturbances affecting the harrow are totally random they are hard to recreate. A similar behaviour can, however, be created. By comparing the data the large underlying disturbance is apparent in both, with the biggest difference being that the simulated output has a fixed sample time while the real output varies a little. Looking at the higher frequency disturbances, the largest peaks in the real data, mainly occurring on the yellow sensor, are not present in the simulations. The reason for this is because these are considered as outliers and are unnecessary to model. When looking at the zoomed in graphs to the right, both have a very similar behaviour. The entire graph, on the other hand, shows some differences between the data. The main difference is that the offset between the four sensors are smaller in the simulated data. The reason for this is how the model is created and the fact that all signals are based on the same disturbance. This is however not considered to be an issue since the signals are being processed later on.

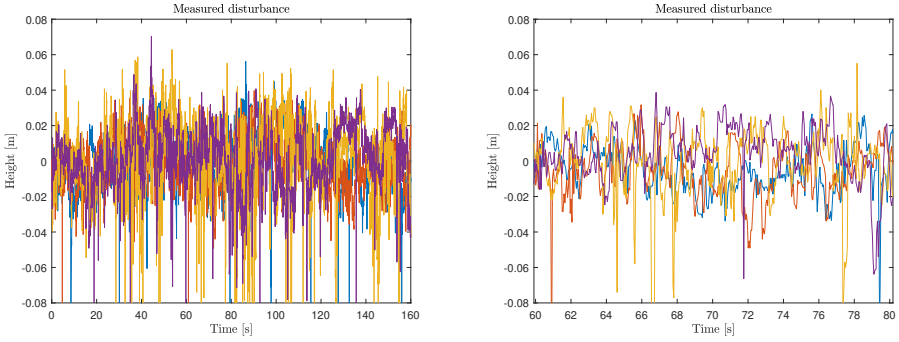

Figure 2.18: *Data gathered from four sensors during a real test.*

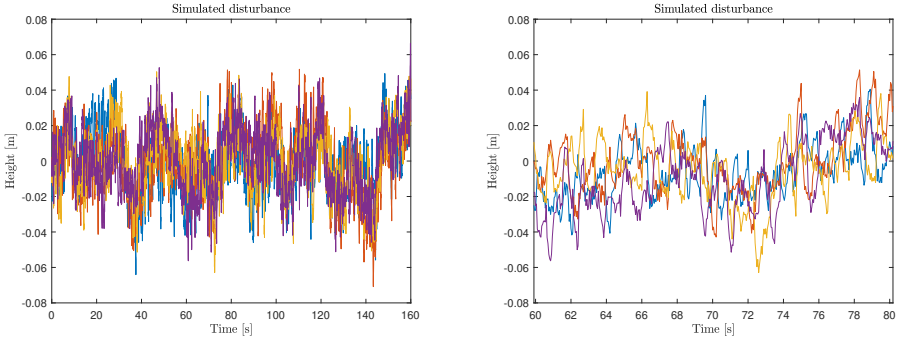

Figure 2.19: *Simulated data representing four sensors.*

3

Sensors and Filtering

This chapter describes the sensor setup on the harrow as well as the proposed filtering strategies. Moreover, suitable filtering strategies for this process and the number of sensors needed to get a satisfying result are discussed.

3.1 Sensors Overview

The sensor used on the harrow is a radar sensor with millimeter precision. It is a 60 GHz pulsed radar that calculates the distance by measuring the time from when a pulse is sent to when the echo is received and has a maximum update rate of 1500 Hz. In total there are nine sensors mounted on the harrow, four measuring the height, two on each crossboard measuring wall height, and one measuring the spring back of a tine.

Height

The four sensors measuring the height are mounted on the main frame of the harrow, one in the middle and three towards the rear of the harrow. The sensors in the rear are mounted, one on each side and one in the center. The sensors are pointed straight down measuring the distance to the ground. The placement on the rear of the harrow gives a more accurate representation of the soil behind the harrow, i.e the result after harrowing.

Tine

The sensor measuring the spring back of the tine is mounted on the main frame pointing straight down measuring the "flat" surface of the tine, illustrated in Figure 3.1. This sensor is used to get an understanding of the actual depth of the tines.

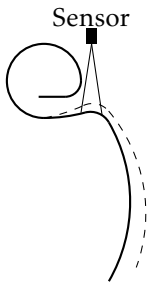

Figure 3.1: *Illustration of how the springback of a tine is measured.*

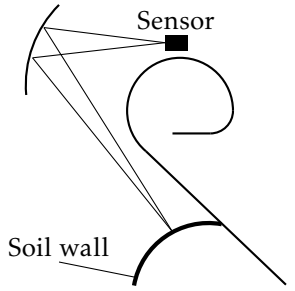

Figure 3.2: *Illustration of how the height of the wall is measured.*

Crossboard

The signal created by the radar has an angle rather than being a straight line. Because of this angle, pointing the sensor directly towards the soil wall resulted in a relatively big radar surface. A big radar surface together with the characteristics of the soil wall did not yield proficient results. Instead the sensor is mounted on the axis which rotates the crossboard itself. It is pointing at a surface shaped as a part of a circle, redirecting the signal in such a way that the radar surface area is minimized. This is illustrated in Figure 3.2.

3.2 Filter Theory

The raw data from the radar sensors contain not only the true distance that is measured, but also different disturbances. These disturbances can be in the form of sensor noise, uneven soil, bias in the placement of the sensors, or dust and debris. To get the desired information from the sensors, the data needs to be filtered and fused. This will provide an estimate of the true value of the measured state.

Given N sensors that measure one state x, each measurement can be modeled as,

$$y_n = h_n(x) + e_n \tag{3.1}$$

where y_n is the measured value from sensor n, $h_n(\cdot)$ is the sensor model and e_n is the measurement error which contains all sources of measurement errors. The goal is to find the best state estimation $\hat{x}$, i.e $\hat{x}$ s.t $y_n \approx h_n(\hat{x})$ for all $n = 1, ..., N$.

In this thesis, two different approaches will be investigated. The first one is a low pass filter with an average over sensors. The idea is that the low pass filter will eliminate the high-frequency disturbances and then take the average between all N sensors, thus compensating for bias and uneven soil. The other approach is to use a more sophisticated filter, the Kalman filter.

3.2.1 Low Pass Filter

The low pass filter (LP) is defined in the frequency plane. The main concept is to let frequencies below a certain limit pass unaltered while frequencies above this limit are removed completely. This limit is called the cut-off frequency, ω_c. The ideal LP filter where all frequencies above the limit are completely removed is not realizable in real-world applications. Instead, the goal is to dampen these high frequencies as much as possible. [4]

The time-discrete transfer function of the first order LP filter is defined as

$$H(q) = \frac{1 - p_{LP}}{q - p_{LP}} \tag{3.2}$$

where q is the forward shift operator, and p_{LP} is the pole of the filter. The cut-off frequency is then defined as,

$$\omega_c = \frac{1}{T} \arccos\left(\frac{-1 + 4p_{LP} - p_{LP}^2}{2p_{LP}}\right). \tag{3.3}$$

Using (3.2), the filtered data from each sensor n can be expressed as,

$$\hat{x}_{n,k} = H(q)y_{n,k} \tag{3.4}$$

By taking the average over all sensors, the estimated state $\hat{x}_k$ from the LP filter will be

$$\hat{x}_k = \frac{1}{N}\sum_{n=1}^{N} \hat{x}_{n,k}, \tag{3.5}$$

where N is the number of sensors.

Delay

One drawback of filtering the measured data is that it introduces a phase delay into the system [4]. This phase delay is defined as the shift of phase between the input and the output of the filter. Consider the frequency function of the filter as $H(e^{i\omega})$. The phase of the function is then defined as

$$\phi(\omega) = \arg H(e^{i\omega}). \tag{3.6}$$

If the input to the filter is a pure sinusoidal $u(t) = \cos(\omega t)$ the output will be

$$y(t) = |H(e^{i\omega})| \cos(\omega t + \phi(\omega)), \tag{3.7}$$

i.e the resulting signal is a pure sinusoidal with a change in amplitude as well as a shift in phase. This shift $\phi(\omega)$ is defined as the phase delay. The delay in phase can be converted to time delay as

$$t_\omega = \frac{-\phi(\omega)}{\omega}. \tag{3.8}$$

For the LP-filter (3.2), the time delay increases with the pole, i.e lower cut-off frequency yields larger time delay. In Figure 3.3 the Bode diagram of three different LP filters is shown. The corresponding time delays for each LP filter when the input is a pure sinusoidal with $\omega = 1\text{rad}/s$ are shown i Table 3.1.

Table 3.1: *Time delay for a signal with frequency 1* rad/*s*.

ω_c [rad/s]	t_ω[s]
1	0.8029 *s*
4.5	0.2601 *s*
14.5	0.0960 *s*

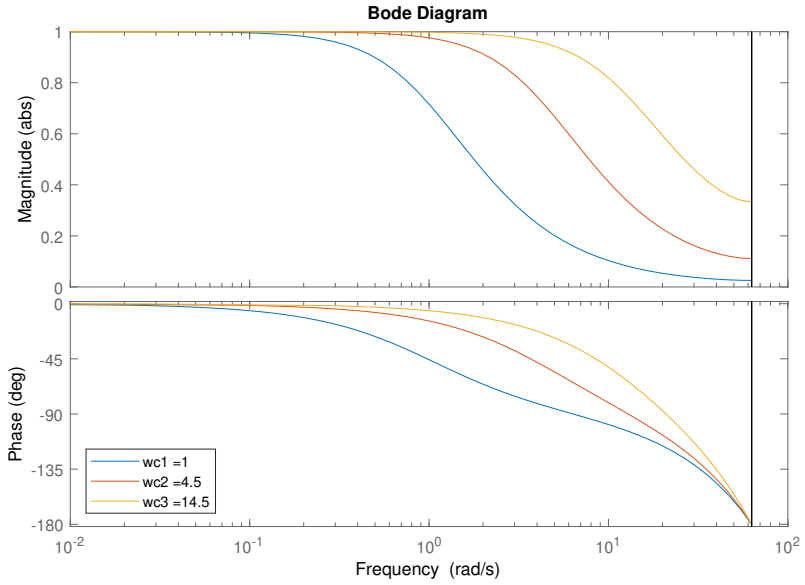

Figure 3.3: *Comparison between low pass filters with three different poles.* $p_{LP,1} = 0.95$ *with* $\omega_c = 1$rad/*s*, $p_{LP,2} = 0.8$ *with* $\omega_c = 4.5$rad/*s*, $p_{LP,3} = 0.5$ *with* $\omega_c = 14.5$rad/*s*

3.2.2 Kalman Filter

The Kalman filter (KF) is an optimal filter for linear sensor models and Gaussian noise that uses the underlying dynamics of the estimated states [5]. KF uses these dynamics together with the measurements to estimate the state. Given that the measured state is from a dynamic process, it can be written as a discrete state space model

$$x_{k+1} = Fx_k + G_u u_k + G_v v_k \tag{3.9a}$$

$$\mathbf{y}_k = Hx_k + Du_k + \mathbf{e}_k, \tag{3.9b}$$

where k is the current time step, u_k is the input signal to the system and v_k is the process noise, including disturbances and model error. Using this model, the KF is defined in two parts. First a so-called time update where the state of the next

time step is predicted, with the motion model

$$\hat{x}_{k|k-1} = F\hat{x}_{k-1|k-1} + G_u u_k \tag{3.10a}$$

$$P_{k|k-1} = FP_{k-1|k-1}F^T + G_v Q_k G_v^T, \tag{3.10b}$$

where P is the covariance matrix of the estimated state $\hat{x}$, and Q_k is the covariance matrix of the process noise v_k. The second step is a measurement update where the estimated state of the next time step is corrected with information from the measurements. The measurement update has the form

$$\hat{x}_{k|k} = \hat{x}_{k|k-1} - K_k\epsilon_k \tag{3.11a}$$

$$P_{k|k} = P_{k|k-1} - K_k S_k K_k^T \tag{3.11b}$$

where

$$\epsilon_k = \mathbf{y}_k - H\hat{x}_{k|k-1} \tag{3.12a}$$

$$S_k = H_k P_{k|k-1} H_k^T + R_k \tag{3.12b}$$

$$K_k = P_{k|k-1} H_k^T S_k^{-1}, \tag{3.12c}$$

and where R_k is the covariance matrix of the measurement error.

Constant Velocity Model

When the dynamic model is not known, or hard to find, a simple solution is to estimate that the state changes with a constant speed between each time step

$$x_{k+1} = \begin{bmatrix} 1 & T_s \\ 0 & T_s \end{bmatrix} x_k + \begin{bmatrix} \frac{T_s^2}{2} \\ T_s \end{bmatrix} v_k. \tag{3.13}$$

This is called a constant velocity (CV) model [3]. Here the state vector x is extended with the velocity, the input of the system is not a controlled signal but the process noise v_k, and T_s is the sampling time of the discrete system.

Delay

The delay that is introduced by the Kalman filter originates from the uncertainty of the model. If the model is not true to the system, the prediction in (3.10a) will be incorrect, and such deviations are partly captured by v_k in (3.9a). These errors are then corrected with measured data in (3.11a). Depending on the covariance matrix Q_k, the filter will trust the model more or less. More trust in the model will introduce more time delay until the filter has corrected for this error, while less trust in the model will result in a signal with higher frequency components.

3.3 Filter Development

The development of the filters started with collecting data from live runs of the harrow. This raw data was then used to test and develop the different filters offline.

3.3.1 Data Collection

The filter data was collected in the beginning of the spring, as soon as the frost and snow thawed. This data collection served the purpose of getting a good understanding of the different sensors, record the movement dependent on the control signal. The main reason was, however, to collect data that could be used to develop the filters.

Each run consisted of one documented movement, which could for example be "change the height of the harrow every twenty seconds" or "change the angle of attack of the front crossboard each 30 seconds". The data from one of these runs are shown in Figure 3.4 - 3.7. In this specific run, the height of the harrow was changed at 20, 40, 140, and 160 seconds, most clearly seen in Figure 3.6.

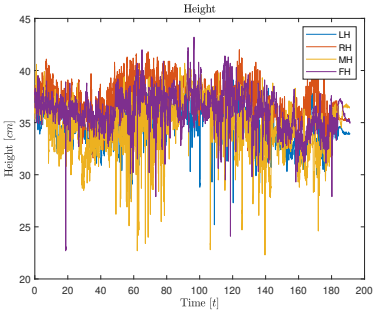

Figure 3.4: *Data from all four height sensors.*

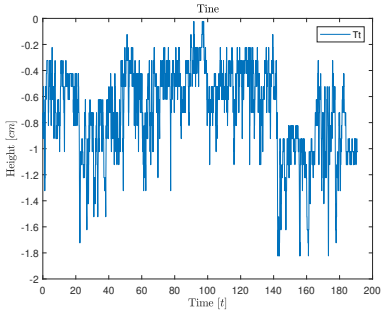

Figure 3.5: *Data from the measured spring back of the tine.*

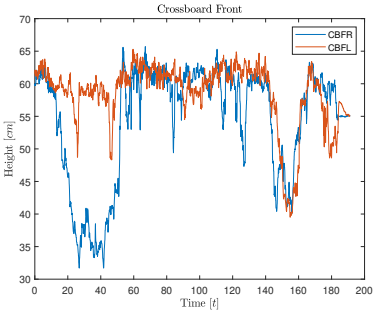

Figure 3.6: *Data from the two sensors measuring the distance between the sensor and the front crossboard wall.*

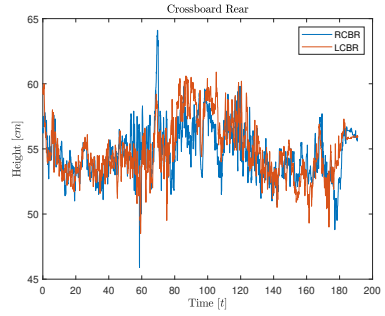

Figure 3.7: *Data from the two sensors measuring the distance between the sensor and the rear crossboard wall.*

3.3.2 Filter Result

Using the measurements from the data collection the LP filter and the KF were designed to best fit each function of the harrow. For the LP filter, the pole p_{LP} can be seen as a design variable. For the KF the covariance of the model error, Q_k can be seen as a design variable. These variables were tuned to satisfy two main criteria. The first one is to dampen the higher frequency noise in the signal, originating from disturbances and measurement errors. The second criteria is to minimize the phase delay that the filters create since delays in the control loop will destabilize the system. In Figure 3.8 a KF and a LP filter are applied to the data from Figure 3.4. The filters have been designed to both have similar phase delays. The biggest difference between the two filters is that the KF manages to dampen higher frequencies while predicting a higher value than the LP filter. The reason why KF predicts a higher value than LP is because that it takes the variance of each sensor into account while predicting the state and since the data from sensor "MH" differs from the other sensors the KF calculation puts less emphasis on that measurement.

Worth noting is that even if conclusions can be drawn from these figures, the actual ground truth of the estimated state is unknown. This creates uncertainties in the comparison and the conclusions should be seen more as qualified estimates.

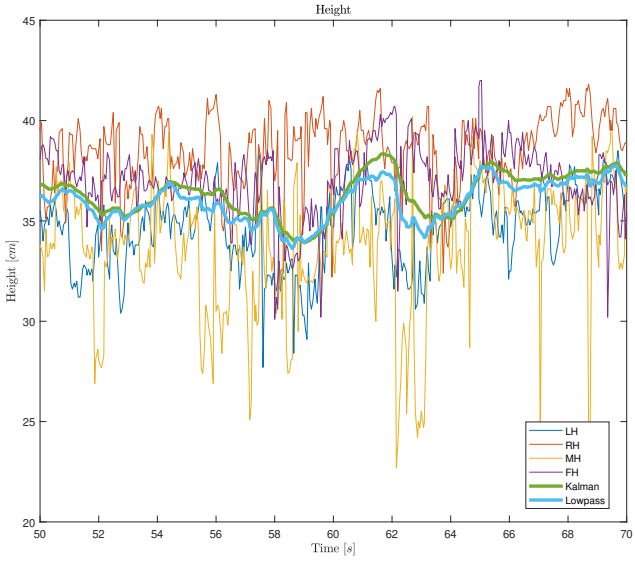

Figure 3.8: *Comparison between Kalman filter and low pass filter on the height sensors with similar phase delays.*

One additional advantage of the the KF is that, in addition to being a filter, the Kalman filter is also an observer [9]. Thus it has the ability to estimate states

that are not measured directly. By using the CV-model (3.13), the KF predicts the rate of change and the possibilities exist to extend the model to predict more states. These states are necessary in order to develop more advanced controllers like the LQ controller [9].

The filter that was chosen to implement on the harrow was the Kalman filter with a CV-model. This filter was chosen due to the possibilities of further development and the superior performance compared with the LP-filter.

4

Control strategy

This chapter describes the theory and development of the algorithms that will control the harrow. It will also investigate the performance of more advanced controllers that requires further development of the harrow.

4.1 Control Introduction

The control algorithm on the harrow will control the harrowing depth and the crossboard walls. The first decision to make is whether it will be controlled by a single multivariable controller or multiple single variable controllers per function. Since the harrow is highly modular when the customer places an order, with possibilities to change, for example, the size and number of crossboards, it is intuitive to have a modular controller as well. In other words, it should be possible to exclude one of the controllers and tune each function to suit the farmer.

The goal is to find the best controller in terms of development cost, system characteristics, and robustness with respect to measurement noise and model errors, as formulated in the problem statement. To do this, the approach is to first develop the most basic feedback controller, the PID-controller, in the simulation environment. This controller is then compared to more advanced control algorithms to decide on which algorithm to implement on the harrow for further testing and analysis.

4.1.1 Requirements

In order to design a suitable control algorithm, some requirements need to be defined. The company has provided information about how a desirable control system should behave. For example, the reference depth for the tines should be

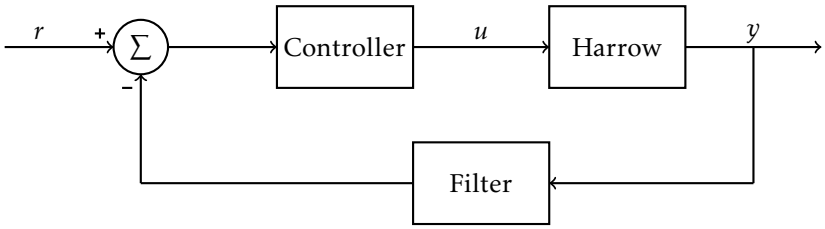

Figure 4.1: *A simplified overview of how the system is structured where r is a reference signal, u is the control signal to the valves and y are the measurements from the sensors.*

between 3-6 cm, the desirable wall should be between 15-30 cm, the optimal controller should not deviate more than 0.5 cm in depth and 5 cm in wall height, and most importantly the system needs to look trustworthy, thus not have a nervous behavior.

From these desires the system requirements are defined as:

- The mean control error of the tine depth d_{tine} should be less or equal to 0.5 cm.
- The mean control error of the crossboard wall height w_{CB} should be equal to or less than 5 cm. The soil wall should never disappear, thus the height should never be 0 cm.
- The normalized total movement of the hydraulic cylinder should be minimized in order to look robust and trustworthy.

The requirements indicate that is will be a trade-off between the control error compensation and the movement of the cylinder.

4.2 Control Theory

4.2.1 PID

A basic Proportional-Integral-Derivative controller, PID-controllerl, uses the error e to create a control signal u. The control signal is used to control a system that creates some kind of observable signal y. The observed signal y is fed back to the controller which computes the error $e = r - y$, where r is a reference. A proportional controller simply lets the control signal be a function of this error according to:

$$u(t) = K_P e(t) + u_0, \tag{4.1}$$

where u_0 is a normal setting for the control signal [11]. The proportional gain controls the speed of the system with a larger K_P resulting in a faster system. While a P-controller would work on its own it can normally not eliminate a disturbance

entirely and a static error can occur. By integrating e, static errors can be determined and eliminated. Hence, by adding an integral term to (4.1) a PI-controller is created as follows:

$$u(t) = u_0 + K_P e(t) + K_I \int_0^t e(\tau) d\tau, \tag{4.2}$$

where the integrating gain K_I determines the speed at which the error is eliminated. Using a PI-controller the control signal can be kept at a desirable value for different disturbances. If, however, a fast system is desired, increasing K_P and K_I will eventually result in instability and self-oscillation [11]. The reason for this is that the proportional and integral terms only uses the size of the error to determine the control signal. By using a derivative term, changes to the error can be taken into account before they fully appears. This is achieved by using the rate of change of the error to determine the control signal. All three terms together create a PID-controller as follows:

$$u(t) = K_P e(t) + K_I \int_0^t e(\tau) d\tau + K_D \frac{d}{dt} e(t), \tag{4.3}$$

where the derivative increases stability and reduces overshoots enabling the system to be fast and accurate.

Continuous to Discrete

When creating a control system the physical system is almost always described in continuous time while the controller, which is implemented digitally, needs to be described in discrete time. One solution to this is to describe the controlled system with a discrete model. The continuous controller described in (4.3) can be rewritten to discrete time by replacing the integral with a sum and the derivative with a difference:

$$u_k = u_0 + K_P e_k + K_I \sum_{i=1}^{k} e_i T_s + K_D \frac{e_k - e_{k-1}}{T_s} \tag{4.4}$$

Tuning

Tuning a PID-controller is highly dependent on the system and application because all systems differ somewhat. Because of this, there is no actual right or wrong way of finding a good tuning and thus no set of parameters that are "right". The work in [2] was motivated by the need to produce tuning parameters obtaining a well-performing PID within agricultural machinery. The FOLIPD model, which is described in (2.9), is covered therein. It motivates different tuning strategies which are discussed and compared. The paper presents a new tuning approach that introduces a minimization problem where several nonlinear

objective functions are optimized simultaneously. For a more in depth description of the tuning approach see [2]. The proposed parameters developed using this method are:

$$K_P = \frac{10^{f(T_d,T)}}{KT_d}, \quad K_I = 0, \quad K_D = \frac{T^{g(T_d,T)}}{K} 10^{h(T_d)} \tag{4.5}$$

where

$$\begin{aligned} f(T_d, T) &= 0.0027(T/T_d)^2 - 0.0794T/T_d - 0.34 \\ g(T_d, T) &= 0.02 + \Big(0.51 - 0.076\log_{10}(T)\Big)T_d^{0.15} \\ h(T_d) &= 0.97 - 1.48T_d^{0.15}. \end{aligned}$$

This optimization covers a wide range of the parameters T and T_d. It does, however, only consider values which ratio T/T_d remains within $[0.1, 10]$. Note that the integral gain is zero which was the case in other methods described in the paper. In conclusion this tuning method outperformed other known methods for this kind of process.

Gain Scheduling

When tuning a controller it might become apparent that a desirable behaviour is hard to achieve in all operating points. If the system has an unstable behaviour due to its characteristics or disturbances the proportional and integrating gains needs to be small. This can however result in a slow system which often is far from ideal. This problem can be addressed by using a predefined set of different gains dependent on the size of the error, known as *gain scheduling*. Using gain scheduling the controller can yield a fast behaviour when the error is big and a more stable behaviour when the error is small.

Feed Forward

If a disturbance is measurable it is possible to use this information as an addition to a controller, known as feed forward. By using a feed forward, the effect of the disturbance can be counteracted before it is visible in the output signal. This does however require an accurate model in order to predict how the disturbance affects the system. [1]

The closed system in Figure 4.2 can be described by:

$$Y(s) = \frac{G_1G_2F}{1 + G_2G_1F}R(s) + \frac{G_2(H + G_1F_f)}{1 + G_2G_1F}V(s) \tag{4.6}$$

where the aim is to eliminate the disturbance V. This is achieved either by choosing a feed forward F_f which minimizes the numerator or by letting the loop gain G_2G_1F be large. An ideal feed forward is obtained using

$$H + G_1F_f = 0 \implies F_f = -\frac{H}{G_1}, \tag{4.7}$$

which completely eliminates the disturbance. However, when using a feed forward the transfer function F_f needs to be stable, causal and proper which means the ideal feed forward might not be usable. In this case one would instead use

$$F_f = -HG_1^\dagger, \tag{4.8}$$

where $G_1^\dagger$ is an approximated inverse to G_1 [1].

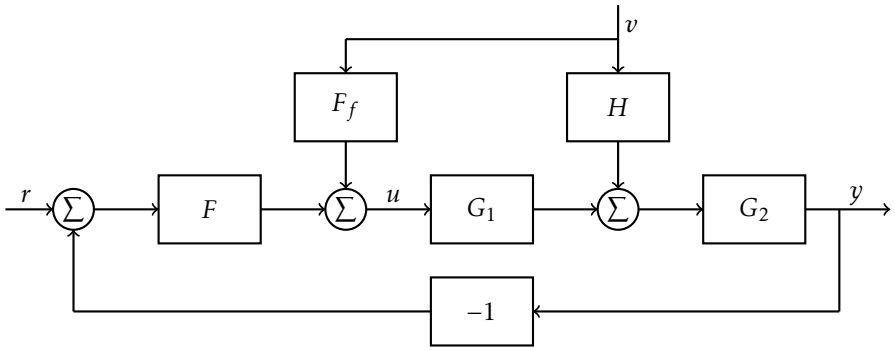

Figure 4.2: *Illustration of how a disturbance v is implemented in a controller with feed forward.*

Cascade Control

When multiple different signals are controlled, there is a possibility to use cascade control to compute the control signals. The basic setup of a cascade controller is illustrated in Figure 4.3. The process is split into two systems where the signal z from the first system is measurable and z is fed back to a controller creating a secondary loop. The advantage with this setup is that disturbances on the system G_1 are immediately taken care of by F_2, which reduces their impact on y. A requirement for cascade control to be advantageous is that the dynamics of the secondary, inner, loop is faster than the dynamics of the primary, outer, loop [1].

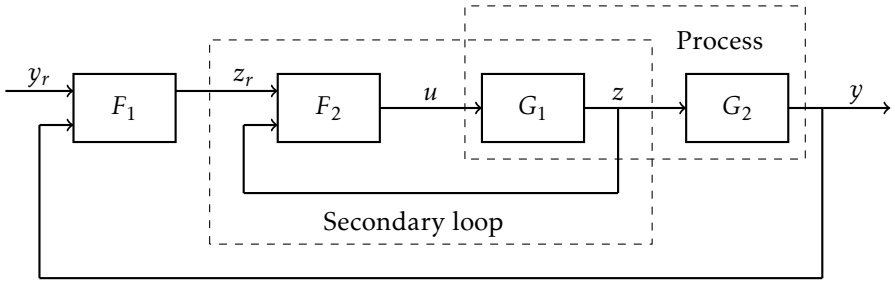

Figure 4.3: *Illustration of the setup of cascade control. The outer loop is the primary.*

4.2.2 Linear–Quadratic Controller

The linear-quadric (LQ) controller is an optimal state-space controller [9]. Given a system model in time-discrete state-space form

$$x_{k+1} = Fx_k + Gu_k + Nv_{1,k} \tag{4.9a}$$
$$z_k = Mx_k \tag{4.9b}$$
$$y_k = Hx_k + v_{2,k} \tag{4.9c}$$

where z is the controlled variable, y is the measured signal, v_1 is process noise and v_2 is the measurement noise. The optimal controller is then defined as the controller which solves the criteria

$$\min_u(\|e\|^2_{Q_1} + \|u\|^2_{Q_2}) = \min_u \sum_{k=0}^{\infty} e_k^T Q_1 e_k + u_k^T Q_2 u_k \tag{4.10}$$

where $e = r - y$, r is the control reference, Q_1 is a semi positive definite weight matrix and Q_2 is a positive definite weight matrix.

If v_1 and v_2 are omitted in (4.9), the control reference is $z = 0$, and if the system is controllable (i.e rank $\begin{bmatrix} G & FG & F^2G & \dots & F^{n-1}G \end{bmatrix} = n$) the optimal controller that solves (4.10) is linear in the form

$$u_k = -Lx_k \tag{4.11a}$$
$$L = (G^T S G + Q_2)^{-1} B^T S F, \tag{4.11b}$$

where S is the positive semidefinite, symmetrical solution to the following matrix equation [9]

$$S = F^T S F + M^T Q_1 M - F^T S G (G^T S G + Q_2)^{-1} G^T S F \tag{4.12}$$

Reference Tracking

If a non-zero control reference ($z \neq 0$) is desired, the controller in (4.11a) can be extended as [9]

$$u_k = -Lx_k + L_r r_k. \tag{4.13}$$

If the dimension of z is equal to the dimension of u, L_r is calculated as,

$$L_r = [M(I + GL - F)^{-1} G]^{-1}. \tag{4.14}$$

This control strategy controls z to the reference value r, and the remaining states to 0.

Linearization

If the system

$$\dot{x} = f(x, u) \tag{4.15a}$$
$$y = h(x) \tag{4.15b}$$

is nonlinear the system needs to be linearized and time discretized in order to use an LQ-controller. Therefore, the system is linearized around a working point x_0, u_0 resulting in a new state, with origin in the working point $\bar{x} = x - x_0$ and $\bar{u} = u - u_0$ [9]. The linearized state-space model is

$$\dot{\bar{x}} = A\bar{x} + B\bar{u} \tag{4.16}$$

where the matrix elements in A and B are

$$a_{i,j} = \left.\frac{\partial f_i}{\partial x_j}\right|_{\substack{x = x_0 \\ u = u_0}}, \qquad b_{i,j} = \left.\frac{\partial f_i}{\partial u_j}\right|_{\substack{x = x_0 \\ u = u_0}}.$$

4.3 Implementation

Using the theory in Section 4.2, the algorithms to control the harrow is implemented using the model data and the filters described in Chapter 3 to satisfy the requirements from Section 4.1. The work flow consists of first developing, testing and comparing algorithms using the simulation environment in Simulink. Then the best performing algorithm in relation to the problem statement are implemented and tested on the real harrow.

4.3.1 PD-controller with Feed Forward

A PID-controller is fairly straightforward to implement in code using the discrete controller described in (4.4). The closed loop in Figure 4.1 was implemented, where the feedback is the filtered signal from the sensors. This setup differs somewhat between the height and crossboards. The basic setup, however, is the same. During early testing it was discovered that the integral term did not improve the controller and it worked just as good without it. This matches the parameter tuning where the integral gain K_I became zero. One of the reasons for this is that the FOLIPD model is an integrating system deems the integral gain unnecessary and thus a PD-controller was implemented for both height and crossboards.

Height

The setup of the closed loop controlling height is almost identical to the structure displayed in Figure 4.1 with the addition of a disturbance. The closed loop from r and v to y is described by:

$$y = \frac{GF}{1 + GF} r + \frac{H}{1 + GF} v, \tag{4.17}$$

where G is a transfer function consisting of the transfer function of the cylinders in (2.9) as well as the state space depth model in (2.28). The controller F was implemented in code according to Algorithm 1 with exception to the feed forward. The signal y is the filtered depth of the tines. The dynamics and vibrations of the tines are considered as a disturbance and a part of v together with the disturbance from the soil in the closed loop.

Crossboard

The closed loop describing the crossboards differs from the height because they are directly affected by the entire harrow. Thus the closed loop is implemented according to Figure 4.2. The closed loop from r and v to y is described by:

$$y = \frac{G_2 G_1 F}{1 + G_2 G_1 F} r + \frac{G_2(H + G_1 F_f)}{1 + G_2 G_1 F} v, \tag{4.18}$$

where G_1 is the transfer function describing the height and the mechanical movement (2.9), (2.15), (2.20), (2.21) and (2.9), (2.15), (2.23) (2.22), (2.24) for front and rear crossboard respectively. G_2 is the transfer function for the state space models describing the soil wall (2.26). The controller was implemented in code according to Algorithm 1 with the implementation of the feed forward presented below. Because of the constraint set for T and T_d mentioned in Section 4.2.1 the optimized tuning is not applicable on the crossboard controllers.

Feed forward

The feed forward added to the crossboards were implemented using the theory described above and (4.6)-(4.8). The signal used in the feed forward is the rate of change of the height produced by the Kalman filter. Since the disturbance affecting the system is the height, H simply becomes an integrator $H = \frac{1}{p}$. The system G_1 can be described by (2.9), (2.15) and (2.21) according to:

$$G_1 = \frac{-L_c \cos(\alpha) \cdot K}{L_a(pT + 1)p}. \tag{4.19}$$

The ideal feed forward therefore becomes:

$$F_f = -\frac{H}{G_1} = \frac{L_a(pT + 1)}{L_c \cos(\alpha) K}, \tag{4.20}$$

which is not proper or causal. Instead an approximated inverse of G_1 is used resulting in:

$$F_f = H G_1^{\dagger} = \frac{L_a(pT + 1)}{L_c \cos(\alpha) K} \cdot \frac{1}{pT^{\dagger} + 1}. \tag{4.21}$$

This transfer function was transformed to discrete time and implemented according to Algorithm 1.

Algorithm 1: PD-controller with feed forward and gain scheduling

input : y, r, $\dot{h}$, $\dot{h}_{-1}$, e_{-1}, u_{f-1}
output: u, u_f, e, $\dot{h}$
$e = r - y$;
if $|e| \leq 0.1$ **then**
  $v_{pos} = K_{P,pos}e + K_{D,pos}\frac{e-e_{-1}}{Ts}$;
  $v_{neg} = K_{P,neg}e + K_{D,neg}\frac{e-e_{-1}}{Ts}$;
else
  $v_{pos} = K_g K_{P,pos}e + K_{D,pos}\frac{e-e_{-1}}{Ts}$;
  $v_{neg} = K_g K_{P,neg}e + K_{D,neg}\frac{e-e_{-1}}{Ts}$;
end
if $v_{pos} > 0$ **then**
  $u = v_{pos} + dz$;
else if $v_{neg} < 0$ **then**
  $u = v_{neg} - dz$;
else
  $u = 0$;
end
if *feedforward* **then**
  $u_f = k_1\dot{h} - k_2\dot{h}_{-1} + k_3 u_{f-1}$;
  $u = u + u_f$;
end

4.3.2 Cascade Control

The cascade controller for the harrow is implemented with the position of the hydraulic cylinder as a secondary loop, inspired by [15]. Since measurements of the hydraulic cylinder are not available on this generation of harrow the cascade controller is at the moment only experimental. This means that the performance will only be investigated in the simulation environment. The cascade controller is fairly similar to the PD-controller, with the exception of the secondary loop and the exception of gain scheduling. The secondary loop, controlling the hydraulic cylinder, is a PD-controller tuned using the tuning rule in (4.5). The main loop is tuned with a PI-controller which was tuned by hand in order to get satisfying results. The cascade controller is implemented according to Algorithm 2.

4.3.3 LQ-controller

The LQ-controller is relatively easy to implement in code. The most complicated part is to calculate the control constants. The LQ-controller uses the estimated states $\hat{x}$ (from the Kalman filter) instead of the "true" states x, a concept known as a LQG-controller [6]. The KF will in other words act as an observer. Using (2.28),

Algorithm 2: Cascade-controller with feed forward

input : y, y_L, r, e_{L-1}, I_{-1}, $\dot{h}$, $\dot{h}_{-1}$, u_{f-1}
output: u, u_f, e_L, I, $\dot{h}$
$e = r - y$;
$I = I_{-1} + K_{I,L} T_s e$;
$r_L = K_{P,L} e + I$;
$e_L = r_L - y_L$;
$v_{pos} = K_g K_{P,pos} e_L + K_{D,pos} \frac{e_L - e_{L-1}}{Ts}$;
$v_{neg} = K_g K_{P,neg} e + K_{D,neg} \frac{e_L - e_{L-1}}{Ts}$;
if $v_{pos} > 0$ **then**
  $u = v_{pos} + dz$;
else if $v_{neg} < 0$ **then**
  $u = v_{neg} - dz$;
else
  $u = 0$;
end
if *feedforward* **then**
  $u_f = k_1 \dot{h} - k_2 \dot{h}_{-1} + k_3 u_{f-1}$;
  $u = u + u_f$
end

linearized (2.29), and (2.30) the control constants L and L_r are calculated using MATLAB. Different control constants are used whether the hydraulic cylinder is expanding or contracting. In Algorithm 3 the LQ implementations are shown. The input is the estimated states $\hat{x}$ and the state control reference r. The output is the applied current to the hydraulic valves u. The constant dz is the dead zone compensation from Figure 2.4. In order to control the crossboards without a steady state error the LQ-controller is extended with an additional state. This state will act as an integral action according to [12], thus eliminating the steady state error.

Algorithm 3: LQ-controller

input : $\hat{x}$, r
output: u
$v_{pos} = -L_{pos} \hat{x} + L_{r,pos} r$;
$v_{neg} = -L_{neg} \hat{x} + L_{r,neg} r$;
if $v_{pos} > 0$ **then**
  $u = v_{pos} + dz$
else if $v_{neg} < 0$ **then**
  $u = v_{neg} - dz$
else
  $u = 0$

5
Results

In this chapter, the results from testing in simulation and on the real harrow will be presented. The first part consist of simulation results. The simulations are focused on two areas. The first one is to decide on which controller that will be implemented on the harrow to do further tests, and the second one is to do tests that are not possible to do on the harrow today. These tests are, for example, experimental controllers, time-consuming tests, and tests with measurements that are not possible to measure on the real harrow.

5.1 Simulation Results

To compare the performance of different control algorithms with each other, several performance indicators are defined:

$$e_{mean} = \frac{1}{N} \sum_{k=1}^{N} |e_k| \tag{5.1a}$$

$$u_{mean} = \frac{1}{N} \sum_{k=1}^{N} |u_k| \tag{5.1b}$$

$$\Delta_L = \int_0^t \left| \frac{dL_c}{dt} \right| dt, \tag{5.1c}$$

where e_{mean} is the normalized mean control error, u_{mean} is the normalized mean control signal and Δ_L is the normalized total movement distance of the hydraulic cylinder. The variable Δ_L will be an indication of nervous characteristics, where more nervousness will lead to longer distances.

5.1.1 Controller Comparisons

The controllers are tested in a 200 seconds long simulation. All simulations were done with the same reference and with the same settings in a Kalman filter with a CV model.

PD-controller with Feed Forward

The PD-controller is suitable to implement on the harrow since it only needs measurements of the depth and wall height. The depth controller is tuned using the optimal tuning rule in (4.5) with some adjustment on the K_p-parameter to have a control signal below the valve saturation. The crossboard controllers were tuned by hand to avoid oscillations and to keep the control signal below the valve saturation. In Figure 5.1, 5.2, 5.3 and Table 5.1 the results from the simulation are presented.

Table 5.1: *Resulting performance indicators from the PD-controller with feed forward.*

Function	e_{mean}	u_{mean}	Δ_L
Depth	0.0059	0.7273	1.265
CBF	0.0535	0.6571	1.435
CBR	0.0370	0.7021	2.172

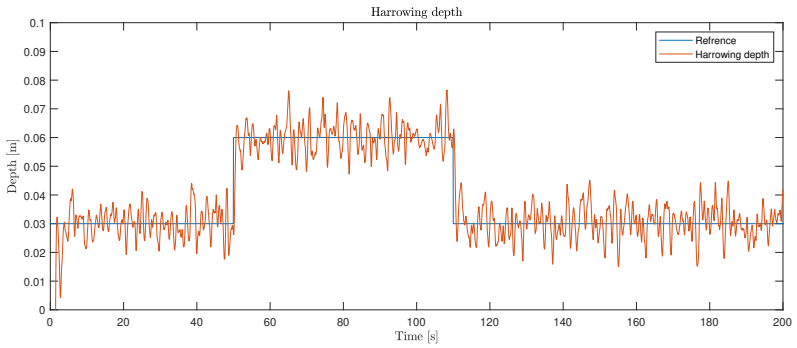

Figure 5.1: *Simulated depth, controlled using a PD-controller.*

In Figure 5.1 it can be observed that the depth oscillates around the reference. This might not look like an undesirable behaviour at first glance, however, the mean error is only about 0.6 cm which is concluded to be an eligible behaviour.

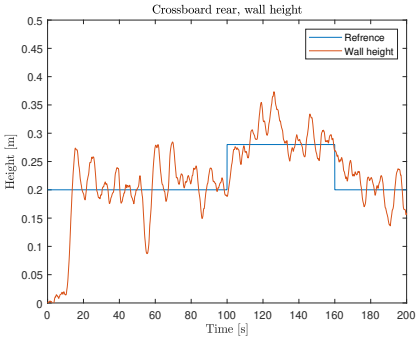

Figure 5.2: *Simulated rear crossboard wall using a PD-controller with feed forward and gain scheduling.*

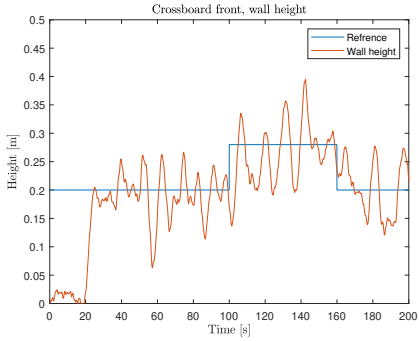

Figure 5.3: *Simulated front crossboard wall using a PD-controller with feed forward and gain scheduling.*

The crossboard is a bigger challenge to control than the depth, mainly since this system is more complex and uncertain. In Figure 5.2 and 5.3 the wall height is oscillating around the reference and has some problems in following the steps in reference, but the mean error is relatively good compared to the control goals.

The feed-forward in the crossboard manages to dampen the disturbance of changing harrowing depth fairly well. The change in depth occurs at 50 and 110 seconds. Some spikes can be observed in Figure 5.2 and 5.3. The controller without feed-forward and gain scheduling can be seen in Figure 5.4 and 5.5. In these simulations one can see significantly bigger spikes at the change in depth. The controller even loses the wall in the front, which is not acceptable.

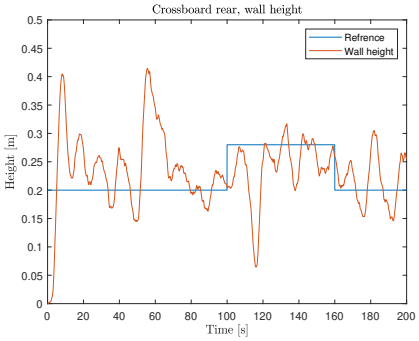

Figure 5.4: *Simulated rear crossboard wall using a PD-controller without feed forward and gain scheduling.*

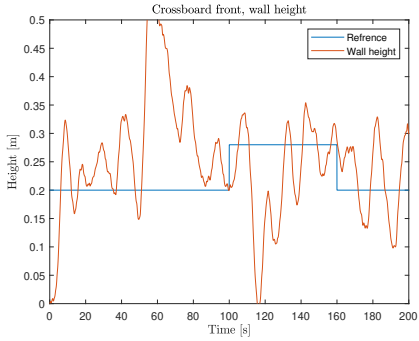

Figure 5.5: *Simulated front crossboard wall using a PD-controller without feed forward and gain scheduling.*

Cascade Controller

Even if the cascade controller is not possible to implement on the harrow, the performance is interesting for further development of the system. The cascade controller is expected to dampen the disturbances, thus being more robust, and minimize the normalized total movement distance. The system was simulated in the same way as the other controllers and the results are shown in Figure 5.6, 5.7, 5.8 and in Table 5.2.

Table 5.2: *Resulting performance indicators from the cascade controller with feed forward.*

Function	e_{mean}	u_{mean}	Δ_L
Depth	0.0062	0.7531	0.950
CBF	0.0533	0.6780	0.888
CBR	0.0506	0.6755	0.642

Comparing Table 5.1 and Table 5.2, the resulting e_{mean} is about the same, but the normalized total movement Δ_L is drastically lowered. Thus showing that the controller manages to control the depth and the wall height using less movement of the cylinder.

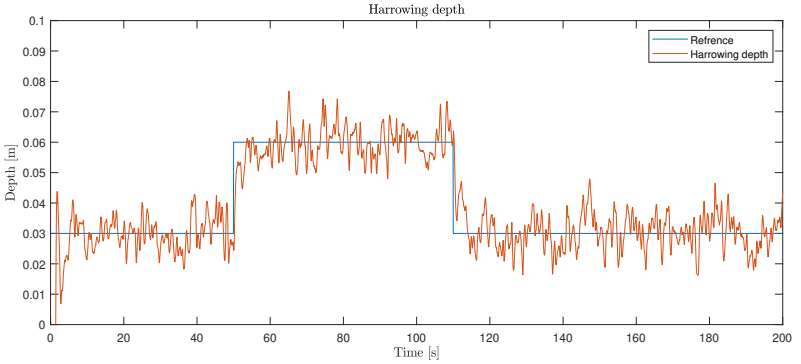

Figure 5.6: *Simulated depth, controlled using cascade control.*

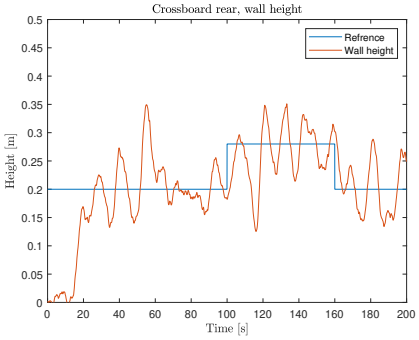

Figure 5.7: *Simulated rear crossboard wall using a cascade controller with feed forward.*

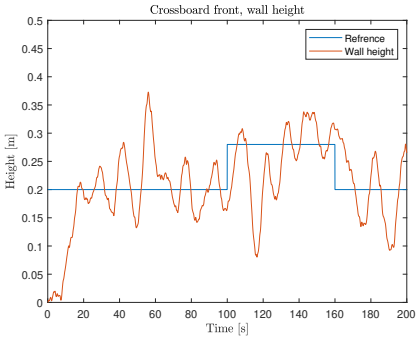

Figure 5.8: *Simulated front crossboard wall using cascade controller with feed forward.*

In Figure 5.6, 5.7 and 5.8, the simulated values are shown. The values never converge and sometimes the error is quite large. But the results are still interpreted as successful since the movement of the cylinder is minimized while the difference in performance is almost not noticeable compared to the PD-controller. In future generations of the harrow, a cascade control system would be suiting.

LQ-controller

The LQ-controller is an optimal controller that is obtained by solving (4.12), but in order to solve this equation, the state-space model needs to be linear and controllable. The state-space model in (2.28) that describes the depth is linear and controllable, thus it is possible to control the depth using an LQ-controller. The controller was implemented and simulated and the resulting simulation is shown in Figure 5.9 and Table 5.3.

Table 5.3: *Resulting performance indicators from the LQ-controller.*

Function	e_{mean}	u_{mean}	Δ_L
Depth	0.0058	0.8096	1.9625
CBF	0.0731	0.6623	0.6588
CBR	-	-	-

Similar to controlling the depth, to control the crossboard wall height using LQ-control the state-space models (2.29) and (2.30) need to be linearized around a working point. In addition to the linearization, the states which represent the cylinder stroke and the cylinder speed needs to be estimated using an observer. The constant velocity model proposed is not enough to estimate these states, therefore the KF needs to be extended with the nonlinear state-space model. Since the original Kalman filter does not support nonlinear models the filter needs to be extended to an extended Kalman filter presented in [3]. As it

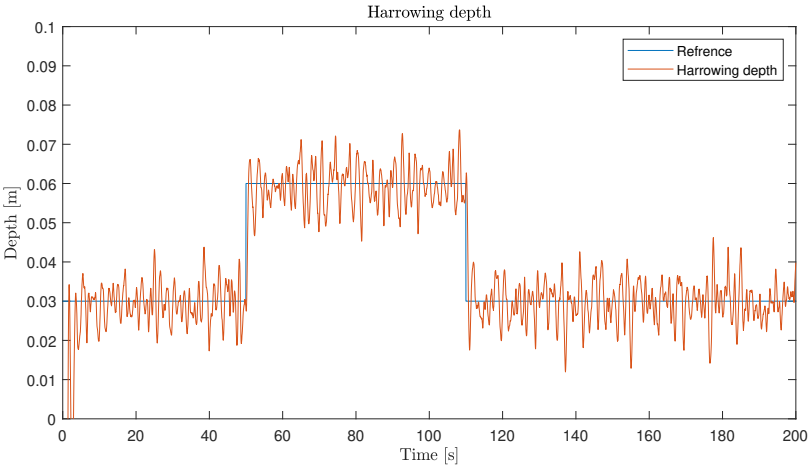

Figure 5.9: *Simulated depth, controlled using a LQ-controller.*

turned out, in order for the extended Kalman filter to estimate the states it needed measurements of the cylinder stroke, thus this controller is not suitable to use on the harrow and is only experimental.

Using the LQ-controller to control the wall it was clear that the algorithm did not manage to follow the reference height. This is because of the model error that is established due to linearization around a working point and the fact that the LQ-controller is only optimal at this exact working point. If this working point is not the equilibrium point of the reference wall height, such that $z = r \nrightarrow \bar{x} = 0$, the states that are not 0 will induce a control signal even if the controlled state is at the reference r. This will intuitively lead to a steady-state error caused by a bias in the linearization error. Since the wall height is not only dependent on the states of the model but also the height of the harrow (v in the model), and that the model is only an approximation of the system, it is impossible to find a linearization point that satisfies $z = r$ and $\bar{x} = 0$. To cope with this error the LQ-controller was extended with an integral action. The performance of this control algorithm on the front crossboard is shown i Figure 5.10 and in Table 5.3.

As can be seen in Figure 5.10 the LQ-controller does not handle the changing height of the harrow well and the results in Table 5.3 is not better than either PD-control or cascade control. Th LQ-controller is therefore not suitable for this application without more advanced modeling.

5.1.2 Filtering

During testing, it became apparent that the choice of filtering parameters had a rather big impact on the behavior and result of the control systems. In the Kalman filter, the ratio between R and Q determines how much the filter relies on measurements versus the model. A larger value of Q resulted in a filter more dependent on the measurements and vice versa. In Figure 5.11 a plot is presented

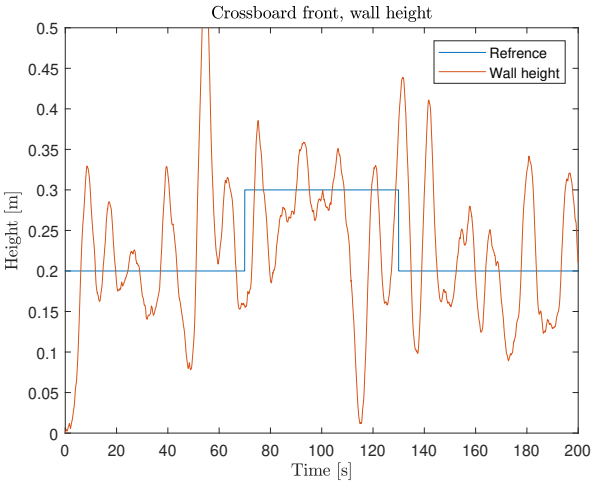

Figure 5.10: *Simulated front crossboard wall height, controlled using LQ control.*

displaying how different values of Q affects the filtered signal. It is apparent that filters relying more on the sensor data have a smaller delay while conversely, relying more on the model results in a smoother signal. Which signal characteristics are best depends on the system. By comparing the results from different filter tuning in Table 5.4 it is shown that the crossboard systems are in greater need of a small time delay while the height performs better when the signal is a bit smoother.

Table 5.4: *Results of how filtering parameters affect the mean error e_{mean}.*

Q	0.1	1	10
Depth	0.0065	0.0059	0.0061
CBF	0.0671	0.0585	0.0521
CBR	0.0812	0.0395	0.0368

5.2 Tests on the Harrow

The control algorithm which was implemented on the harrow was the PD-controller with feed forward and gain scheduling, with the motivation that it only needs measurements of the variables to control, is fairly easy to tune and is a simple controller to implement and to understand.

Using the parameters determined during simulations as a guide, the controller was tuned to best suit the real implementation. One problem that occurred was that the rear crossboard did not work as expected on the real harrow.

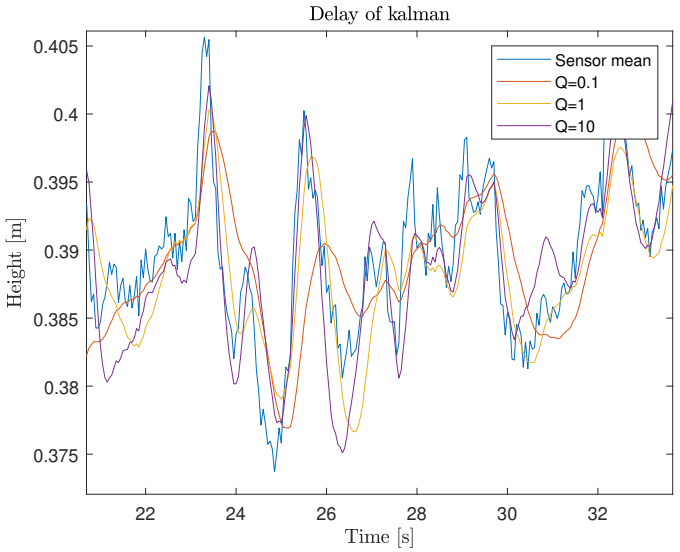

Figure 5.11: *Illustration of how the filtered signal differs depending on Q compared to the mean value of all sensors.*

The rear crossboard did not manage to build a soil wall even with the maximum angle of attack. Therefore, there is no data from the real-world tests of the rear crossboard. The resulting data and performance indicators from the real-life tests can be seen in Figure 5.12, 5.13 and in Table 5.5

Table 5.5: *Resulting performance indicators from the test on the harrow.*

Function	e_{mean}	u_{mean}
Depth	0.0046	0.6616
CBF	0.0387	0.7544

Comparing Table 5.5 with Table 5.1 one can observe that the harrow implementation performs better than the simulation in terms of e_{mean}, with the harrow implementation succeeding to clear the first criteria of the control requirements in Section 4.1.1.

Comparing Figure 5.1 with Figure 5.12 the clear difference of the two plots is the frequency of the signal, which indicates that the simulation environment simulates disturbances with higher frequencies and that the controller applied to the harrow is slower than in simulation.

Comparing Figure 5.3 with Figure 5.13 the first difference is the reference height. The reason for a lower reference height is that during testing, the tractor pulling the harrow could not cope with the force that was created by a larger soil wall. Another difference between the two figures is that the tests on the harrow

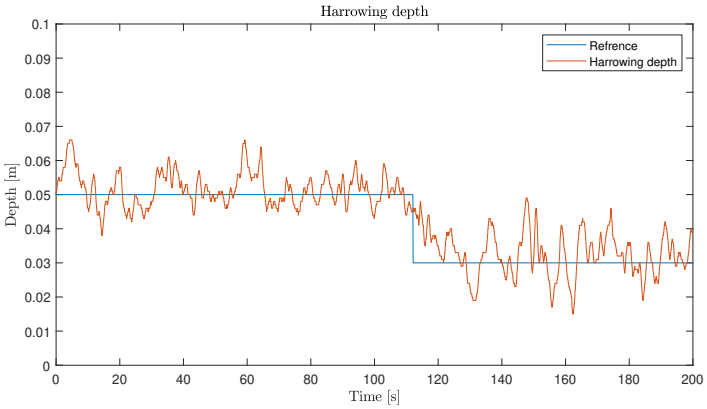

Figure 5.12: *Measured depth from tests on the harrow.*

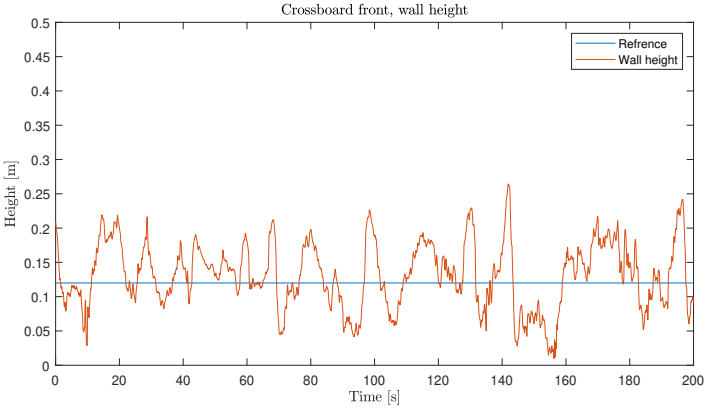

Figure 5.13: *Measured front crossboard wall height from test on the harrow.*

almost lose the wall completely at, for example, 140 s. The reason for this is that the test runs are not straight and during U-turns, the crossboards lose the wall which then needs to be regained.

6

Conclusions

In this thesis, a complete control system for a seedbed tine harrow has been created. This includes modeling the harrow, creating a simulation environment, designing a filter strategy, and creating and comparing different control algorithms. This resulted in a control system that managed to live up to all requirements.

In this chapter, conclusions are drawn based on the Problem statement, Section 1.1.3, presented in Chapter 1. Strengths and weaknesses of different control and filter strategies are covered as well as future development which can be done to the software and hardware.

6.1 Conclusions

Advanced control strategies require more sophisticated models of the real system. A simple controller can cope with a coarse model, while the restrictions of the system and simple movement patterns are sufficient. However, in order to design a more advanced system a thorough description of the dynamics is needed. An accurate and realistic model is especially important when testing is costly and time-consuming as in this work. The ability to simulate in a realistic environment saves both time and money and results in a more robust control system because more tests can be carried out.

Likewise, the necessary measurements and the choice of filtering strategy are dependent on the complexity of the control system. For simple controllers only measuring the controlled variable is sufficient and only when using more advanced structures, like cascade control, the need to measure several variables increases. However, because of the large size of the harrow, even a simple controller can benefit from several measurements of the same variable. The choice of filter strategy is of great importance, both large noise and time delay are unwanted characteristics from the filter. When choosing and tuning the filter a trade-off

had to be made because more aggressive filtering results in a bigger time delay, and once again, the different systems required different filter tuning. The choice of filter strategy is also dependent on the controller, where a more basic low pass filter can produce the same result as the more complex Kalman filter. However, the Kalman filter creates more flexibility because it can be used to estimate unmeasured states, which makes it possible to use more advanced control strategies, for example, feed-forward and LQ.

With the current setup of the harrow the best-performing control strategy considering development cost, system characteristics and robustness is a PD-controller with feed-forward to the crossboards as it is a relatively simple yet efficient system. Better performance can be obtained by using measurements of the stroke of the cylinder to create a cascade controller. However, this requires additional sensors which result in larger development costs. An LQ-controller was also tested, which in theory is an optimal controller for linear systems. This strategy does, however, require an exact model for it to perform optimally. Because the system the controller was applied on is nonlinear and the disturbances are unpredictable it is not fit for use without a more advanced disturbance modeling.

6.2 Future Work

The proposed PD-controller can be developed into a cascade controller. In simulations this has been shown to increase performance regarding the smoothness of the system. While maintaining a reference tracking equal to that of the PD, the cylinder movement decreases a lot. This is desirable because it decreases wear on joints and is perceived by the customer as a less nervous system, which is positive. A cascade controller is easy to implement in code but the system needs additional sensors measuring the position of the cylinder stroke.

During the final testing, it was observed that the front crossboard had a tendency to build up a larger soil wall in the middle of the harrow. Because of the placements of the two sensors measuring the wall, they did not measure the build-up in the middle and therefore the controller did not compensate for this. For future development of the system more sensors should be installed, at least one in the middle. More sensors measuring the height could also result in better performance especially if the system is implemented on larger harrows.

The control system is created in a modular way which provides the opportunity to split systems, keeping in mind future implementation on larger harrows. The crossboard could be split into sections working independently of each other which would result in a more evenly sized soil wall across the whole width of the crossboard. The same principle could be applied to the wheels letting the height be controlled separately. This would be especially applicable to larger harrows because they cover a wider area with more varying soil.

A potential system that has not yet been researched or tested in this thesis is a pressure-controlled crossboard. Rather than controlling the position of the cylinder stroke, hence the crossboard angle, this controller would control the oil

pressure in the cylinder system. This system would be able to control itself because the crossboard would give in if the soil wall grew too big resulting in a force exceeding the oil pressure. However, a controller and radar sensors measuring the height of the wall would still be needed, but it could result in better performance.

Appendix

A

Simulink model

Here follows a presentation of the Simulink model used to simulate the harrow.

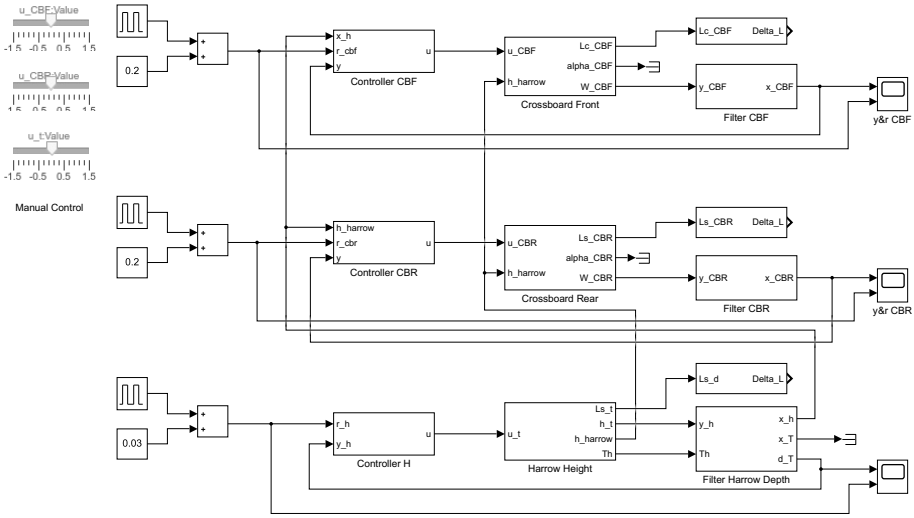

Figure A.1: *The complete model for simulating the harrow. One block for control, one for motion and one for filtering per function.*

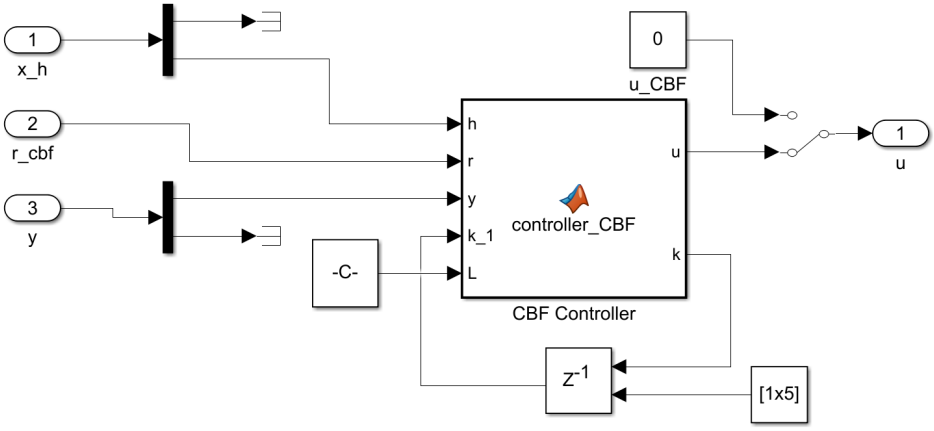

Figure A.2: *How the controller of the front crossboard is simulated, the other functions are controlled in a similar way.*

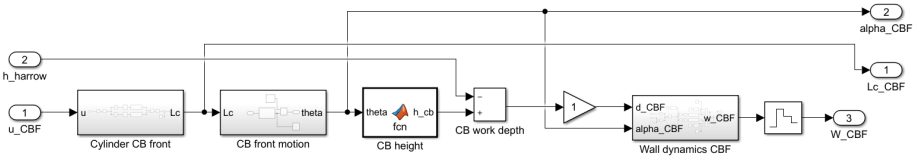

Figure A.3: *How the motion of the controller front crossboard is simulated. Each function is simulated in a similar way.*

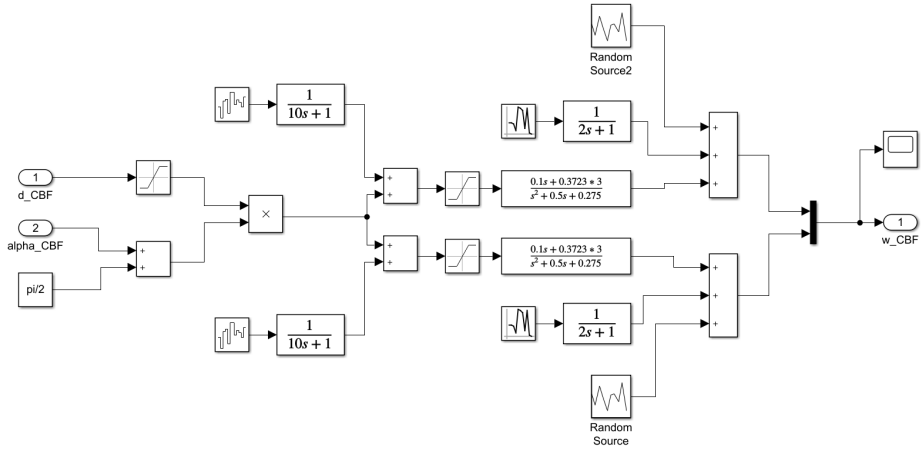

Figure A.4: *How the wall dynamics is simulated. Each crossboard is simulated in a similar way.*

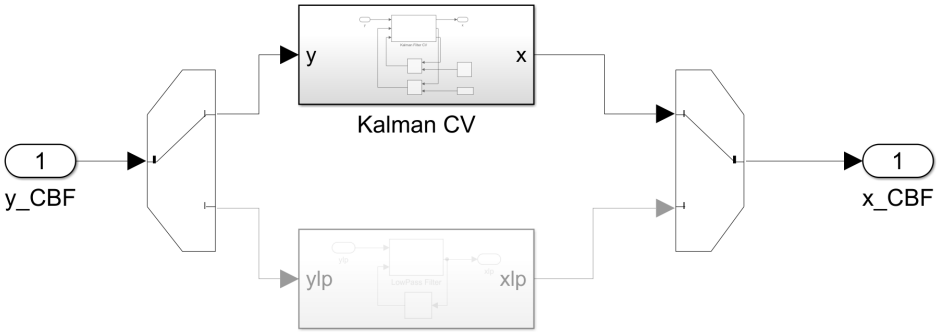

Figure A.5: *How the filter of the front crossboard is simulated, each filter is simulated in a similar way.*

Bibliography

[1] Martin Enqvist, Torkel Glad, Svante Gunnarsson, Peter Lindskog, Lennart Ljung, Johan Löfberg, Tomas McKelvey, Anders Stenman, and Jan-Erik Strömberg. Industriell reglerteknik kurskompendie. Course literature in Industrial control applications at Linköpings University. Printed at the university., jan 2014.

[2] L Eriksson and T Oksanen. Pid controller tuning for integrating processes: analysis and new design approach. In *Proc. Fourth International Symposium on Mechatronics and its Applications, harjah, UAE*, 2007.

[3] Fredrik Gustafsson. *Statistical sensor fusion*. Studentlitteratur, Lund, third edition edition, 2018. ISBN 9789144127248.

[4] Fredrik Gustafsson, Lennart Ljung, and Mille Millnert. *Signal processing*. Studentlitteratur, Lund, första upplagan edition, 2010. ISBN 9789144058351.

[5] R. E. Kalman. A New Approach to Linear Filtering and Prediction Problems. *Journal of Basic Engineering*, 82(1):35–45, 03 1960. ISSN 0021-9223. doi: 10.1115/1.3662552. URL https://doi.org/10.1115/1.3662552.

[6] R. E. Kalman et al. Contributions to the theory of optimal control. *Bol. soc. mat. mexicana*, 5(2):102–119, 1960.

[7] Jeyong Lee, M Yamazaki, A Oida, H Nakashima, and H Shimizu. Electrohydraulic tillage depth control system for rotary implements mounted on agricultural tractor design and response experiments of control system. *Journal of Terramechanics*, 35(4):229 – 238, 1998. ISSN 0022-4898. doi: https://doi.org/10.1016/S0022-4898(98)00026-3. URL http://www.sciencedirect.com/science/article/pii/S0022489898000263.

[8] Lenart Ljung. System identification toolbox, 2021. URL https://se.mathworks.com/help/ident/.

[9] Lennart Ljung and Torkel Glad. *Reglerteori Flervariabla och olinjära metoder*. Studentlitteratur AB, second edition, 2003.

[10] Lennart Ljung and Torkel Glad. *Modellbygge och Simulering*. Studentlitteratur AB, second edition, 2004.

[11] Lennart Ljung and Torkel Glad. *Reglerteknik: Grundläggande teori*. Studentlitteratur AB, fourth edition, 2006.

[12] MathWorks. Linear-quadratic-integral control, 2021. URL https://se.mathworks.com/help/control/ref/ss.lqi.html.

[13] Satyam Paul, Ajay Arunachalam, Davood Khodadad, and Olena Rubanenko. *Fuzzy Tuned PID Controller for Vibration Control of Agricultural Manipulator*. IEEE, 2020. ISBN 978-1-7281-9352-6. doi: 10.1109/HORA49412.2020.9152848. URL http://urn.kb.se/resolve?urn=urn:nbn:se:oru:diva-84882.

[14] Andrew J Scarlett. Integrated control of agricultural tractors and implements: a review of potential opportunities relating to cultivation and crop establishment machinery. *Computers and Electronics in Agriculture*, 30(1):167 – 191, 2001. ISSN 0168-1699. doi: https://doi.org/10.1016/S0168-1699(00)00163-0. URL http://www.sciencedirect.com/science/article/pii/S0168169900001630.

[15] Pasi Suomi and Timo Oksanen. Automatic working depth control for seed drill using iso 11783 remote control messages. *Computers and Electronics in Agriculture*, 116:30 – 35, 2015. ISSN 0168-1699. doi: https://doi.org/10.1016/j.compag.2015.05.016. URL http://www.sciencedirect.com/science/article/pii/S0168169915001520.